63-3-3

Report 1456

DEPARTMENT OF THE NAVY
DAVID TAYLOR MODEL BASIN

HYDROMECHANICS

AERODYNAMICS

STRUCTURAL MECHANICS

APPLIED MATHEMATICS

EFFECT OF AXIAL POSITION OF PROPELLER ON THE PROPULSION CHARACTERISTICS OF A SUBMERGED BODY OF REVOLUTION

by

John L. Beveridge

HYDROMECHANICS LABORATORY
RESEARCH AND DEVELOPMENT REPORT

March 1963 Report 1456

EFFECT OF AXIAL POSITION OF PROPELLER ON THE PROPULSION CHARACTERISTICS OF A SUBMERGED BODY OF REVOLUTION

by

John L. Beveridge

March 1963

Report 1456
S-R009 01 01

TABLE OF CONTENTS

LIST OF FIGURES

LIST OF TABLES

NOTATION

DIMENSIONAL QUANTITIES

A	Cross-sectional area of a body of revolution
A_e	Expanded area of propeller blades
A_0	Propeller disk area
D	Maximum diameter of a body of revolution
d	Propeller tip diameter
L	Length of a body of revolution
L_0	Distance aft of reference station
l	Blade section length
n	Propeller frequency of revolution
P	Propeller pitch
P_e	Effective or tow rope power
P_s	Shaft power
p	Local static pressure excluding hydrostatic pressure
p_v	Vapor pressure
p_∞	Static pressure at infinity
Q	Propeller torque
q	Free-stream stagnation pressure, $\frac{1}{2}\rho V^2$
r, θ, w	Spherical coordinates
R	Radius of a propeller blade section, or radius in general
R_B	Maximum radius of a body of revolution
R_h	Propeller hub radius
R_j $(j = f, r, t)$	Resistance
R_0	Propeller tip radius
S	Wetted surface
T	Propeller thrust
U	Total fluid velocity
v_a	Propeller slip velocity at infinity
u_i	Propeller-induced velocity tangent to the body surface
u_t	Potential velocity on body surface without propeller

V	Undisturbed fluid velocity, or body speed
V_a	Axial velocity of propeller or pitot tube through the water
v	Propeller section inflow velocity
$v_r = -\frac{\partial \phi}{\partial r}$	Disturbing velocity along the radius vector
$v_\theta = -\frac{1}{r}\frac{\partial \phi}{\partial \theta}$	Disturbing velocity normal to the radius vector
X, Y	Rectangular coordinates
Z	Number of propeller blades
$\frac{\partial \Gamma}{\partial X}$	Circulation distribution
ρ	Mass density
ϕ	Velocity potential

COEFFICIENTS AND RATIOS

	FORMULA	
$\frac{A_e}{A_0}$		Propeller expanded blade-area ratio
C_f	$R_f/\frac{1}{2}\rho S V^2$	Frictional-resistance coefficient
C_p	$2\pi Q n/\frac{1}{2}\rho\pi \frac{d^2}{4} V_a^3$	Propeller power coefficient
C_r	$R_r/\frac{1}{2}\rho S V^2$	Residual-resistance coefficient
C_T	$T/\frac{1}{2}\rho \frac{\pi d^2}{4} V_a^2$	Propeller thrust-load coefficient
C_t	$R_t/\frac{1}{2}\rho S V^2$	Total-resistance coefficient
$\frac{d}{D}$		Propeller-body diameter ratio
e_h	$\frac{1-t}{1-W_0}$	Hull efficiency
e_p	$K_t J/2\pi K_q$	Propeller efficiency
e_r		Relative rotative efficiency
J	V_a/nd	Propeller speed coefficient
K_t	$T/\rho n^2 d^4$	Propeller thrust coefficient

K_{td}	K_t/J^2	Propeller thrust-load coefficient
K_q	$Q/\rho n^2 d^5$	Propeller torque coefficient
$\frac{P}{d}$		Propeller pitch ratio
$\frac{p}{q}$	$p/\frac{1}{2}\rho V^2$	Pressure coefficient
$\frac{R}{R_B}$		Radius fraction
$\frac{R}{R_0}$		Radius fraction
$\frac{r}{R}$		Radius fraction
t	$1 - \frac{R_t}{T}$	Thrust-deduction coefficient or thickness
W	$1 - \frac{V_a}{V}$	Wake fraction
W_0		Taylor or effective wake fraction
x, y	$\frac{X}{L}, \frac{Y}{D}$	Dimensionless coordinates
β_i		Hydrodynamic pitch angle
δ		Angle of tangent line to body of revolution
ϵ		Section drag-lift ratio
η_p		Propulsive coefficient
σ_x*		Cavitation number

*Subscript x is used to denote a local value.

ABSTRACT

The propulsion performance of a submerged body of revolution was determined when the axial clearance between a stern propeller and the body was varied. Theoretical and experimental results indicate that variations, within the range of investigation, in the longitudinal position of a stern propeller do not critically affect the propulsive coefficient. In addition to these results, calculation of the propellers and the thrust deduction is discussed, and experimental results obtained from numerous wake traverses are presented.

INTRODUCTION

As part of the Bureau of Ships Fundamental Hydromechanics Research Program, the David Taylor Model Basin is studying the problem of propulsion interaction. Propulsion interaction effects for a single propeller and for counterrotating propellers on deeply submerged bodies of revolution have been the subject of previous investigations.[1,2,3,4] Weinblum[5] in his paper on thrust deduction has concisely set forth the physical nature of the propulsion interaction problem. In a general manner he described some of the theoretical methods used in calculation of thrust deduction and indicated the state of recent scientific knowledge. Breslin showed, in Reference 2, the dependence of the thrust deduction upon the slope of the sectional area curve at the stern of a body of revolution. He also found the variation of thrust deduction (for a given size propeller) with axial clearance for an ellipse of revolution having the same fineness ratio as a hypothetical arrangement of the airship AKRON. Korvin-Kroukovsky[1] calculated the wake fraction and thrust deduction for AKRON when a hypothetical stern propeller installation is specified. Historically, a great deal more experimental work has been done on the propulsion interaction problem as associated with surface ships than has been done on submerged bodies. However, considerable theoretical work has been accomplished which deals with the various aspects of the interaction problem for the case of axisymmetric flow. Emphasis on theoretical work in this direction is because the axisymmetric flow case is more amenable to mathematical treatment.

Each of the aforementioned papers has contributed considerably to the available information on the subject of marine propulsion; however, the present study differs in several particulars from the investigations just cited. In addition to the determination of thrust deduction and wake, the total propulsive coefficient is considered with emphasis on obtaining the best propeller efficiency for a given set of operating conditions. This is extended to give the performance of propellers as related to the axial spacing between propeller and body. A Series 58 form was used for the experiments and the computed example. This report includes model propulsion test results and presents and discusses necessary wake surveys, thrust deduction determination, open-water data, and propeller calculations.

---

[1]References are listed on page 47.

STATEMENT OF PROBLEM

Propulsion characteristics of a submerged body are determined by the performance of a body and propeller system. The body affects the propeller performance through its wake and the body resistance is affected by the induced velocity field of the propeller. The general problem is to find in what way the propeller is influenced by the body, and conversely, in what way the body is influenced by the propeller. In this report these mutual influences are investigated for a well-streamlined body of revolution when equipped with a stern propeller located at different axial positions. The specific problem treated is to determine the best efficiency, as a function of axial position, of a stern propeller of a given diameter, and then to determine the optimum axial spacing between propeller and body based on propulsive coefficient.

The approach used in this report to reach a solution to this interaction problem may be outlined as follows: The velocity and pressure distribution over the surface of an axisymmetric body without propeller, in potential flow, was obtained by generating the prescribed shape with a surface distribution of sources. The induced velocity field ahead of a propeller was determined by assuming that the propeller may be represented by a cylindrical vortex sheet. The thrust deduction force, i.e., interaction force, was obtained by suitable integration of the pressure distribution over the afterbody with and without a propeller. The inflow to the propeller is mostly viscous in origin; therefore, the wake was experimentally determined at various positions behind a Series 58 form of 7.3 fineness ratio. An optimum wake-adapted propeller was designed for each axial position, using a method in current use at the Model Basin. To investigate the effect of axial position on propeller performance, the propeller thrust and diameter were kept constant. Finally, the approach as outlined permitted the propulsive coefficient to be computed. Experimental confirmation was obtained from tests of one calculated propeller.

Other limitations and assumptions involved in the method may be stated as follows:

1. It is assumed that the propeller-induced velocity normal to the body can be neglected; i.e., the boundary conditions on the body are not met. It is shown that the accuracy of the calculated thrust deduction is not seriously impaired by this neglect for the well streamlined body considered.

2. It is assumed that the fluid is incompressible and inviscid except that the total wake to the propeller is considered; i.e., the problem is treated as a potential one except that a viscous correction is made to the wake. The problem must be treated this way since the effect of a stern propeller on a body of revolution is mainly potential in origin whereas the effect of the body on the propeller is mostly viscous in origin.

ANALYSIS

PRINCIPAL CONSIDERATIONS

To make the theoretical analysis tractable, only a submerged well-streamlined body of revolution was considered. This choice of body shape does not infer that the effects of various appendages and appendage arrangements are not of practical importance.

From a propulsion viewpoint, the performance of any given body and propeller system can be analyzed by means of the propulsive coefficient η_p* and its components. The relation is

$$\eta_p = \frac{P_e}{P_s} = e_h \cdot e_p \cdot e_r$$

where e_h is the hull efficiency $\frac{1-t}{1-W_0}$,

e_p is the propeller open-water efficiency, and

e_r is the relative rotative efficiency.

Consider the components of the propulsive coefficient. First, the hull efficiency e_h is the ratio $\frac{1-t}{1-W_0}$, where $(1 - W_0)$ is the effective wake factor which is experimentally determined and $(1 - t)$ is the thrust deduction factor. It is necessary to obtain wake experimentally inasmuch as the theory of free turbulent shear flow is not developed sufficiently to give reliable results in the near field behind a body. The flow field of the body alone is regarded as composed of two superimposed fields. These two fields are the body velocity V and the disturbance velocity W_0V. If the velocity field of a propeller, which is operating behind a body, is superimposed on the velocity field of the body, the combined velocities produce a pressure gradient which usually reduces the pressure along the afterbody. This pressure reduction augments the resistance of the body so that only part $(1 - t)$, the thrust deduction factor, of the propeller thrust is available to overcome the resistance experienced by the body without propeller. The thrust deduction problem is analogous to the familiar problem of finding the forces between two bodies in a flow field. Unlike the inflow into the propeller, the induced velocity field ahead of the propeller and the body velocity without a propeller can be computed theoretically with sufficient accuracy for the present investigation. Alternatively, a good approximation to the thrust deduction can be obtained experimentally by means of stock propellers. Experimentation of this type is costly, and inasmuch as an adequate theory appears to exist for axisymmetric bodies, it seems preferable to seek a theoretical solution with experimental confirmation at a few points.

---

*The propulsive coefficient should not be used to compare different body shapes.

Second, consider propeller efficiency behind a body. It is apparent that the calculation of an optimum propeller for each axial position behind a body of revolution requires the use of (1) the wake which is obtained experimentally and (2) the thrust deduction which is obtained theoretically. The circulation theory as applied to wake-adapted propellers is used to compute the propeller performance at each axial position. Propeller efficiency for the behind condition is given by the product of open-water efficiency e_p and the so-called relative rotative efficiency e_r. If a wake survey is available, the propeller efficiency for the behind condition ($e_p \cdot e_r$) may be estimated from the relation

$$e_p \cdot e_r = \frac{C_T}{C_p} \approx \frac{\displaystyle\int_{\text{hub}}^{1} \frac{1 - \epsilon \tan \beta_i}{(1 - W_x)^2} \frac{dC_{TSi}}{d\left(\frac{R}{R_0}\right)} d\left(\frac{R}{R_0}\right)}{\displaystyle\int_{\text{hub}}^{1} \frac{1 + \frac{\epsilon}{\tan \beta_i}}{(1 - W_x)^3} \frac{dC_{PSi}}{d\left(\frac{R}{R_0}\right)} d\left(\frac{R}{R_0}\right)} \qquad [1]$$

Next, consider propeller performance in open water. Propeller performance characteristics in open water are of considerable interest particularly, for systematic series and for ship powering estimates where the concept of an equivalent speed of advance is introduced. An effective wake fraction W_0 is determined by this procedure. Making use of an effective wake fraction, propeller open-water efficiency of a wake-adapted propeller can be approximated by the following equation:

$$e_p = \frac{TV_a}{2\pi Qn} = \frac{C_T}{C_p} \approx \frac{1 - W_0 \displaystyle\int_{\text{hub}}^{1} (1 - \epsilon \tan \beta_i) \frac{dC_{TSi}}{d\left(\frac{R}{R_0}\right)} d\left(\frac{R}{R_0}\right)}{\displaystyle\int_{\text{hub}}^{1} \left(1 + \frac{\epsilon}{\tan \beta_i}\right) \frac{dC_{PSi}}{d\left(\frac{R}{R_0}\right)} d\left(\frac{R}{R_0}\right)} \qquad [1a]$$

where the propeller thrust-load and power coefficients C_{TSi} and C_{PSi} are based on ship speed and are for nonviscous flow,

T is propeller thrust,

Q is propeller torque,

V_a is propeller speed of advance,

n is propeller frequency of revolution,

ϵ is the section drag-lift ratio,

β_i is the hydrodynamic pitch angle, and

$\frac{R}{R_0}$ is the radius fraction.

Finally, the relative rotative efficiency is obtained numerically from Equations [1] and [1a] as the ratio of the propeller efficiency in the behind condition to that in open water.

The subsequent sections of the report are chiefly concerned with the details of reaching a solution for and calculating the variation of the propulsive coefficient with axial position of a propeller. The foregoing approach used to find the propulsive components is summarized as follows:

Problem	Method of Solution
Determination of flow due to the body	Experimental wake measurements and calculation of pressure distribution on body.
Determination of the flow ahead of a propeller	Induced velocities due to a cylindrical vortex sheet.
Thrust deduction	Body and propeller flow combined. The appropriate pressures on the hull afterbody then integrated to yield the thrust deduction force.
Propeller efficiency	Circulation theory as applied to wake-adapted propellers using a design method developed by Eckhardt and Morgan.

DETERMINATION OF THRUST DEDUCTION

The addition of the propeller-induced velocities to the velocities at the body produces a reduction in pressure on the body within the field of propeller influence. The difference

$$\Delta R_t = T - R_t$$

where T is the propeller thrust and R_t is the body resistance without a propeller, is variously called the thrust deduction force or resistance augmentation and the ratio $t = \frac{\Delta R_t}{T}$ is known as the thrust deduction coefficient. The thrust deduction will be calculated in this report by pressure integration. The formulation of the solution is two-fold: (1) A propeller field as represented by Korvin-Kroukovsky[1] will be used to obtain the propeller-induced velocities. The component of these velocities, which is tangent to the body, is then combined with the potential velocities u_t at the body surface to yield the total fluid velocity U. (2) The pressure defect Δp on the body due to the working propeller is calculated and then integrated in the x-direction over the afterbody to yield the thrust deduction.

Turn now to the problem of combining the propeller velocity and body velocity fields. Figure 1 diagrams the disturbing velocities due to the propeller and shows schematically a typical body meridian profile and the propeller disk at several locations. The longitudinal

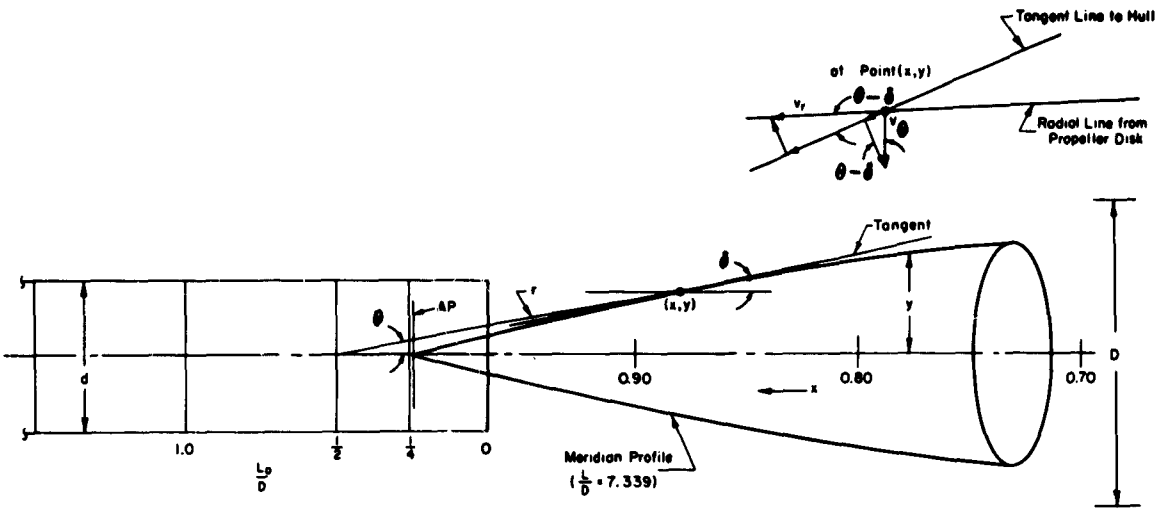

Figure 1 – Schematic Diagram of Body-Propeller Arrangement Showing the Magnitude of Pertinent Velocities

position of each propeller plane is a distance L_0 aft of a so-called reference station at $L_0 = 0$. For the remainder of this report, L_0 is expressed as a fraction of the maximum diameter D of the body. The magnitude of the propeller-induced velocity u_i which is tangent to the body is

$$u_i = v_r \cos(\theta - \delta) - v_\theta \sin(\theta - \delta)$$

and the total fluid velocity U for the body plus propeller is

$$U = u_i + u_t$$

where u_i is the propeller-induced velocity tangent to the body surface,

u_t is the potential velocity on the body surface without propeller,

U is the total fluid velocity,

v_r is the disturbing velocity directed opposite to the radius vector from the propeller,

v_θ is the disturbing velocity normal to the spherical radius vector (positive when directed toward the body axis),

θ is the vectorial angle, and

δ is the angle of inclination of the tangent to a body of revolution.

When $\theta < \delta$, v_θ increases U and, conversely, when $\theta > \delta$, v_θ decreases U. The total value of U for propeller and body must be greater on the afterbody than the value of U for the body alone; i.e., the increase in velocity over the hull afterbody decreases the absolute pressure. A procedure for obtaining the total fluid velocity ratio U/V is formulated in detail in Appendix C.

NUMERICAL COMPUTATIONS AND RESULTS

THRUST DEDUCTION FOR CHOSEN BODY

The pressure distribution, which corresponds to a source-sink distribution for Model 4620 without a propeller, and the combined pressure distributions of this body plus propeller are shown in Figure 2. Calculations leading to the distribution of the pressure field $\Delta \frac{p}{q}$ in Figure 2 are arranged in Tables 4, 5, and 6 of Appendix C for propeller positions $\frac{L_0}{D}$ of 1/4, 1/2, and 1, respectively. It can be seen from Figure 2 that the effect of the propeller field is significant for approximately the last 20 percent of the body length. Propeller-induced velocities normal to the body are neglected; thus, the boundary condition that the normal velocity at a point on the body surface be zero is not satisfied. For the present case, the neglect of this component does not seriously impair the accuracy of the calculated thrust deduction. The following data illustrate the order of magnitude of the pertinent quantities.

	$L_0/D = 1/4$			$L_0/D = 1.0$		
x	v_θ/V	v_r/V	$v_r/V \sin(\theta - \delta)$	v_θ/V	v_r/V	$v_r/V \sin(\theta - \delta)$
0.70	Zero	0.0004	0.00003	Zero		
0.80	↓	0.0009	0.0000	↓	0.0004	0.0000
0.92	↓	0.0054	0.0002	↓	0.0010	−0.0001
0.98	0.004	0.0365	−0.0002	↓	0.0023	−0.0004

Propeller-induced velocity v_θ is seen to be essentially zero and propeller-induced velocity $v_r/V \sin(\theta - \delta)$, which is normal to the tangent line at a point on the body, is also seen to be negligible. When $\sin(\theta - \delta)$ is significant, then v_r is small. Of course, these compensating effects are a result of the streamlined shape of the body under consideration and may not be true in general. The integral in Equation [4] of Appendix C can be computed by Simpson's rule using the slope data of Table 3 (see Appendix C) and the pressure coefficients of Figure 2. Results of evaluating t as a function of L_0/D are shown in Figure 3.

In retrospect the wake and thrust deduction are mutually dependent quantities. Assuming the propeller is an actuator disk, the exact functional relation between t and W in pure streamline flow has been independently derived by several authors.[5,6,7] The relation can be expressed in the following convenient form:

$$1 - W_p = 1 - \frac{t_p}{2}\left(1 + \sqrt{1 + C_T}\right) \qquad [2]$$

The potential velocity ratio $(1 - W_p)$ was computed from Equation [2] by making use of the values of t given in Figure 3 and the nonviscous values of C_T which were computed in

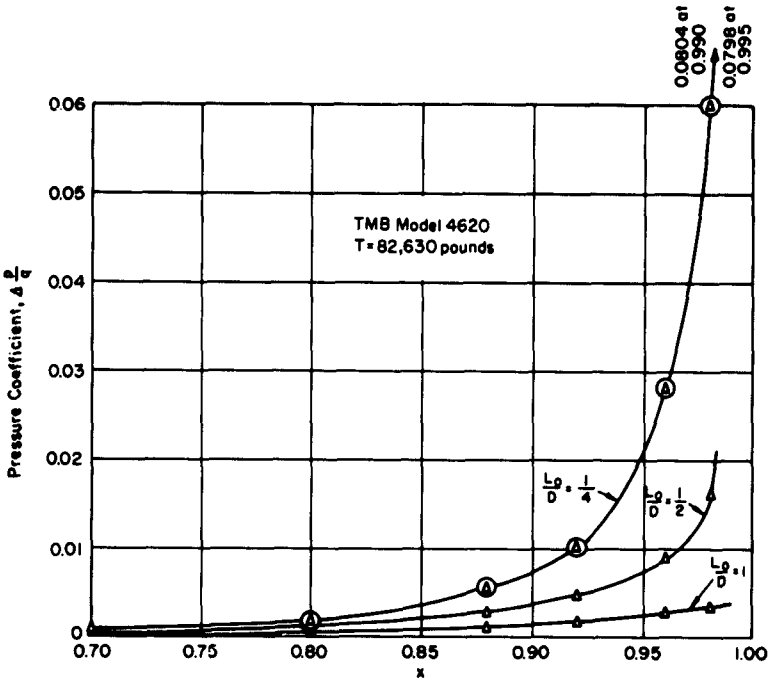

Figure 2a – Differences between Pressure Coefficients for Towed and Propelled Conditions

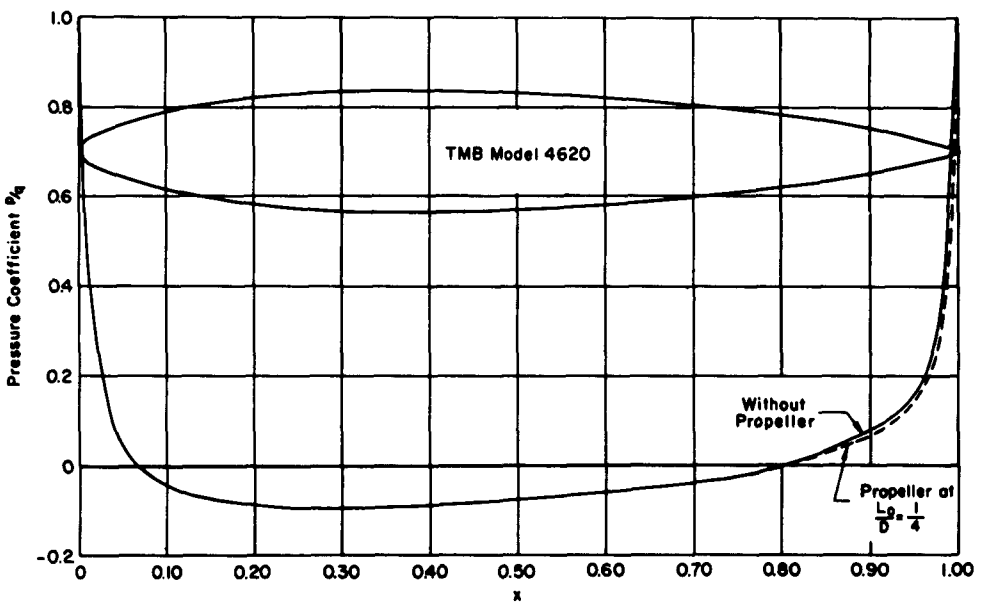

Figure 2b – Pressure Distribution with and without a Propeller

Figure 2 – Pressure Field on Afterbody of Model 4620

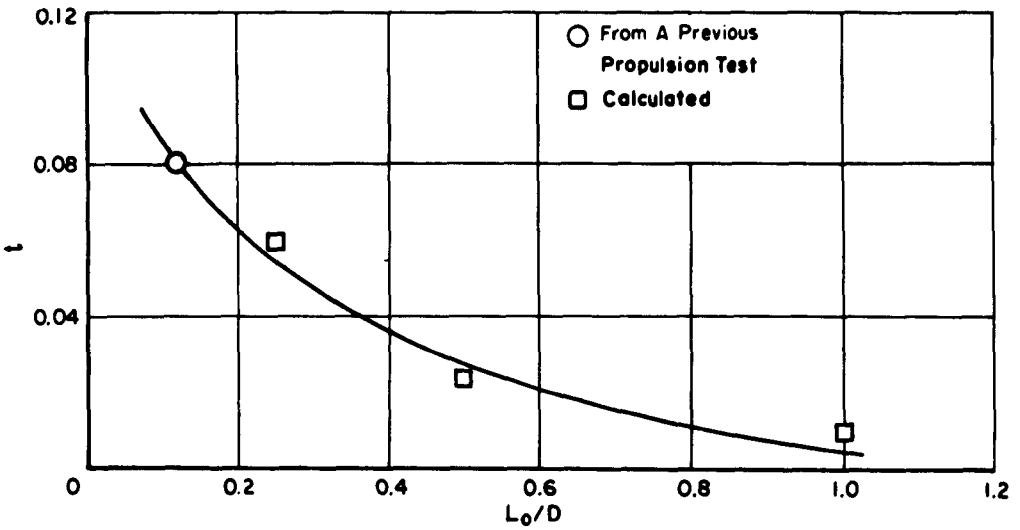

Figure 3 – Thrust-Deduction Coefficient versus L_0/D

connection with the propeller design. Results are plotted in Figure 21 of Appendix D. These comparative data reveal clearly the effect of nonuniform wake and the convergence of the curves at large values of L_0/D.

GEOMETRY AND DESIGN CONDITION FOR EACH PROPELLER

All propellers calculated and tested are five-bladed designs having sections comprised of a thickness form with an NACA 66 nose and a parabolic tail with an $a = 0.8$ mean line. Each propeller was calculated by the circulation or vortex theory using the design method of Eckhardt and Morgan.[8] The approach was to determine the optimum propeller from the standpoint of efficiency for each longitudinal position. Although cavitation is not part of this study, incipient cavitation curves were used to help determine the blade-section chord. To systematically investigate the effect of axial spacing between body and propeller, the most important remaining parameters should remain constant; therefore, to satisfy this requirement both propeller thrust and propeller diameter were fixed. Calculation of a propeller for a specified longitudinal position was based on the radial wake distribution (see Appendix D) and the theoretically obtained thrust-deduction coefficient at that particular transverse station, a constant thrust of 82,630 lb for a 200-ft prototype and a propeller-body diameter ratio d/D of 0.5. The choice of 0.5 for the value of d/D is based on TMB classified data which indicate that $d/D = 0.5$ gives the proper propeller diameter in the present case for the behind condition.

A significant departure from what has been done by most investigators in dealing with the interaction problem is the emphasis placed on a suitable propeller. In this study, an optimum propeller and a nonoptimum propeller, for a given diameter, are determined for the flow and load conditions that exist at each location. The design conditions can now be

formulated, based on the values of $(1-t)$ and $(1-W)$ already determined. The optimum rpm-diameter relationship was determined from Gawn's[9] open-water curves. The results are:

L_0/D	P/d	J	$N_{optimum}$
1/8	1.44	1.16	154.4
1/4	1.51	1.20	153.7
1/2	1.60	1.27	150.8
1.0	1.70	1.36	147.0

Alternatively, e_p and P/d were obtained for a range of rpm, and e_p is plotted in Figure 4. For comparative purposes, a set of four nonoptimum propellers which would operate at a higher and possibly more practical rpm was calculated. These propellers were calculated for 200 rpm, where from Figure 4 it is seen that a drop in e_p of about 6 or 7 points has occurred. The loss in e_p is much more rapid in the range of $N > 200$ and demonstrates clearly the penalty in propeller efficiency for operation at higher rpm for the chosen diameter. Altogether, the performance of nine propellers was theoretically determined, one was built and tested. Table 1 summarizes the design conditions and location of each propeller.

TABLE 1

Summary of Propeller Locations and Design Conditions

$T = 82{,}630 \quad \frac{d}{D} = 0.5 \quad z = 5$

$\frac{L_0}{D}$	150 RPM	200 RPM
0.125	x	x
0.250	x	x
0.500	x	x
0.600	x*	
1.000	x	x

*Propeller 3836. This propeller was built and tested.

Calculations for moderately loaded propellers using Lerbs' induction factors have been programmed on the UNIVAC high-speed digital computer at the Model Basin.[10] The radial distribution of wake fraction that was used in the propeller calculations is presented in Appendix D (see Figure 20), but the nominal wake was corrected by the $\frac{(1-W_0)}{(1-W_{0.7})}$ and replotted to a base of R/R_0 in Figure 5.

Curves of A_e/A_0 versus L_0/D are shown in Figure 23 for $N = 150$ and 200. A final radial distribution of pitch is plotted in Figure 24 (Appendix E) for each propeller at its proper longitudinal position L_0/D. These final pitch curves result from applying appropriate corrections based on methods presently employed at the Model Basin for friction and lifting-line to lifting-surface effects.[8]

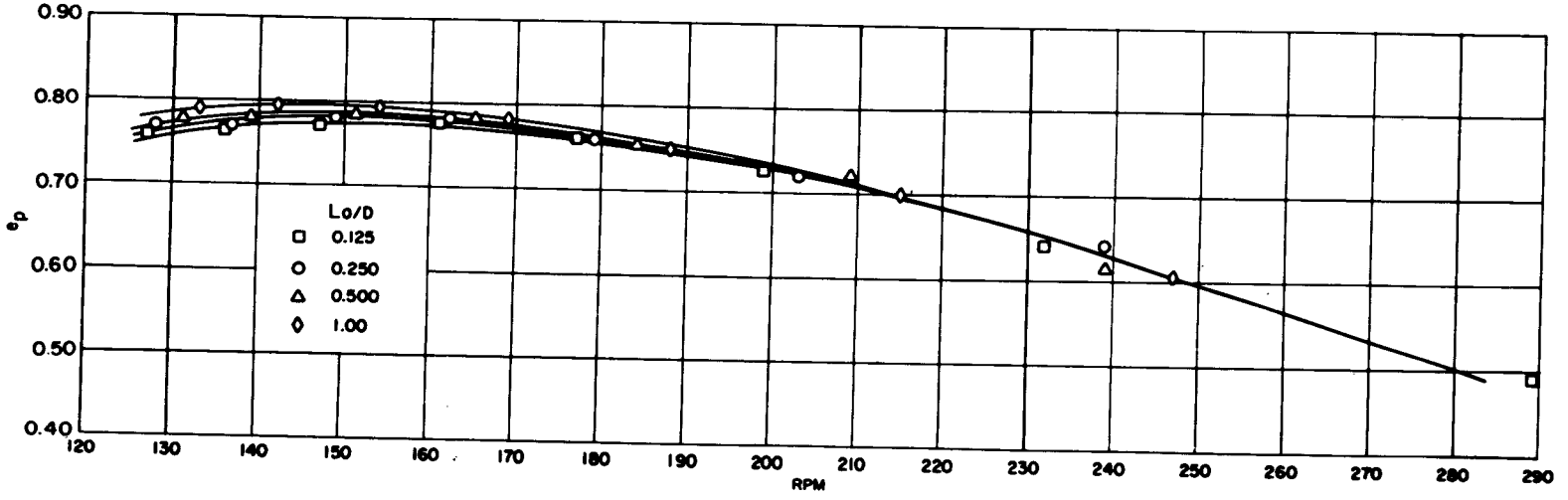

Figure 4 – Propeller Efficiency versus RPM with L_0/D as a Parameter

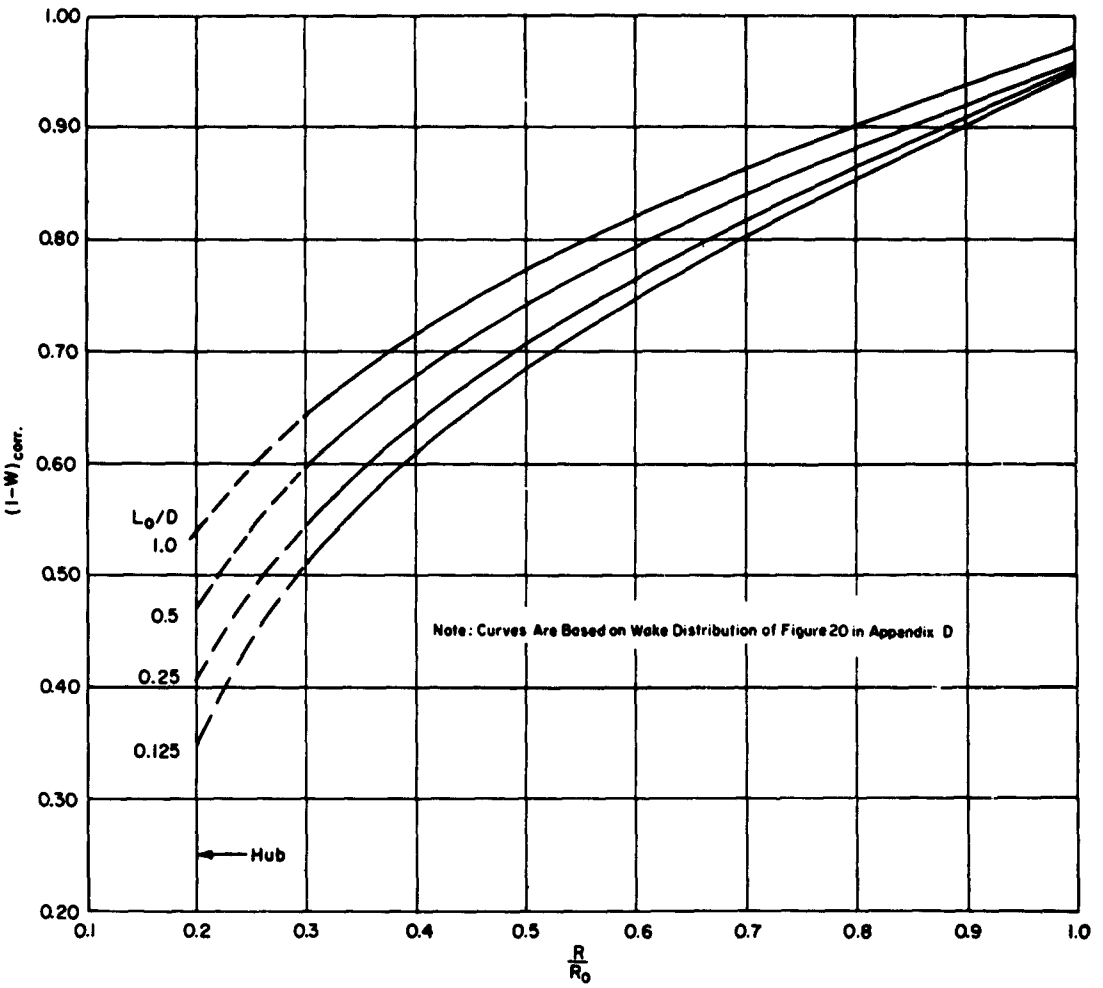

Figure 5 – Curves of Estimated Effective Velocity Ratio versus R/R_0

PROPELLER PERFORMANCE AS RELATED TO SPACING

A computed curve of propeller open-water efficiency versus L_0/D is given in Figure 6 for 150 rpm and 200 rpm. The propeller efficiency was obtained from a numerical solution[8,10] of Equation [1]; see Analysis. Of importance is the variation of the propulsive coefficient η_p with L_0/D. Figure 7 gives an estimated curve of η_p versus L_0/D for optimum propellers where the components in the relation $\eta_p = e_p \cdot e_r \cdot e_h$ are obtained in the following manner: Propeller efficiency ($e_p \cdot e_r$) behind the body is approximated by Equation [1] using local wake fractions from Figure 5. Hull efficiency $e_h = \dfrac{1-t}{1-W_0}$ is estimated by using the thrust deduction data in Figure 3 and by assuming the effective wake fraction as being equal to the wake taken at $R/R_0 = 0.7$ from Figure 5.

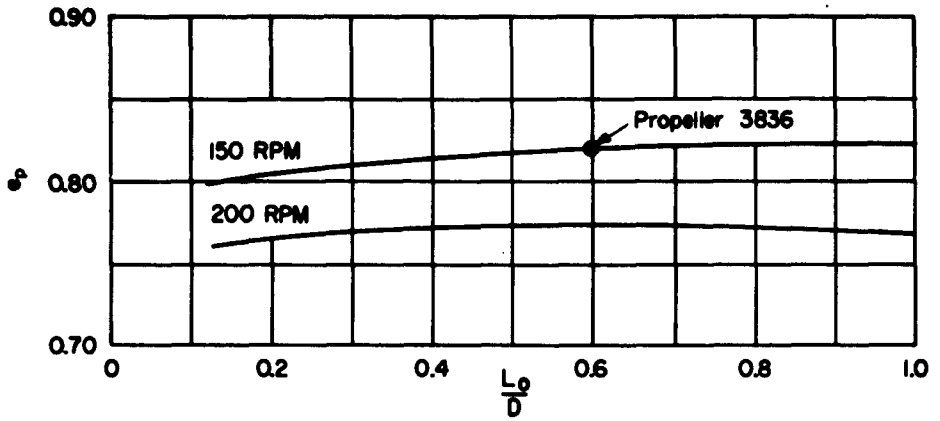

Figure 6 – Propeller Efficiencies Calculated According to Equation]1a]

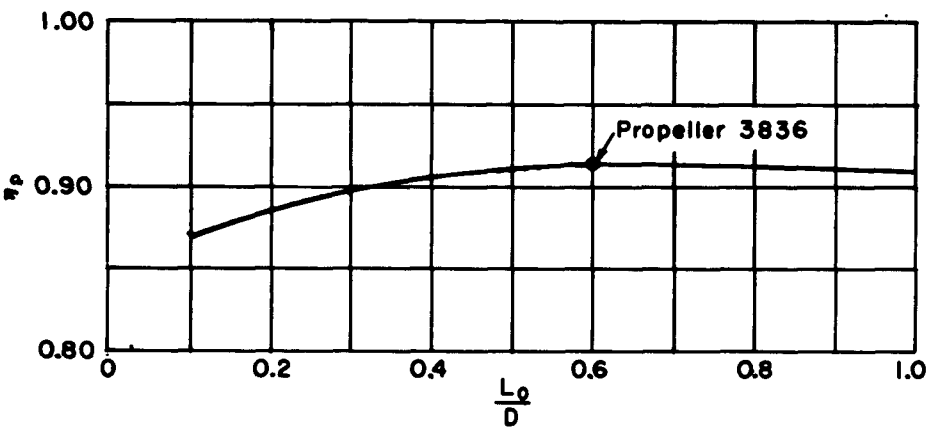

Figure 7 – Propulsive Coefficient versus L_0/D

It seems logical to conclude from Figure 7 that variations, within the range of investigation, in the longitudinal position of the propeller do not critically affect propulsive efficiency. In fact, it appears that there is a broad flat optimum which allows considerable freedom of choice in locating a stern propeller, but a modest increase in η_p seems likely if a propeller is positioned somewhat aft of the reference location.

EXPERIMENTS

To experimentally verify the calculated performance of the optimum propellers, Propeller 3836 was tested in open water and behind the body at $L_0/D = 0.6$. Appendix B contains a description of the salient features of the instrumentation and test procedure. Resistance tests were conducted on the model with the sting extended (see Figure 8) and

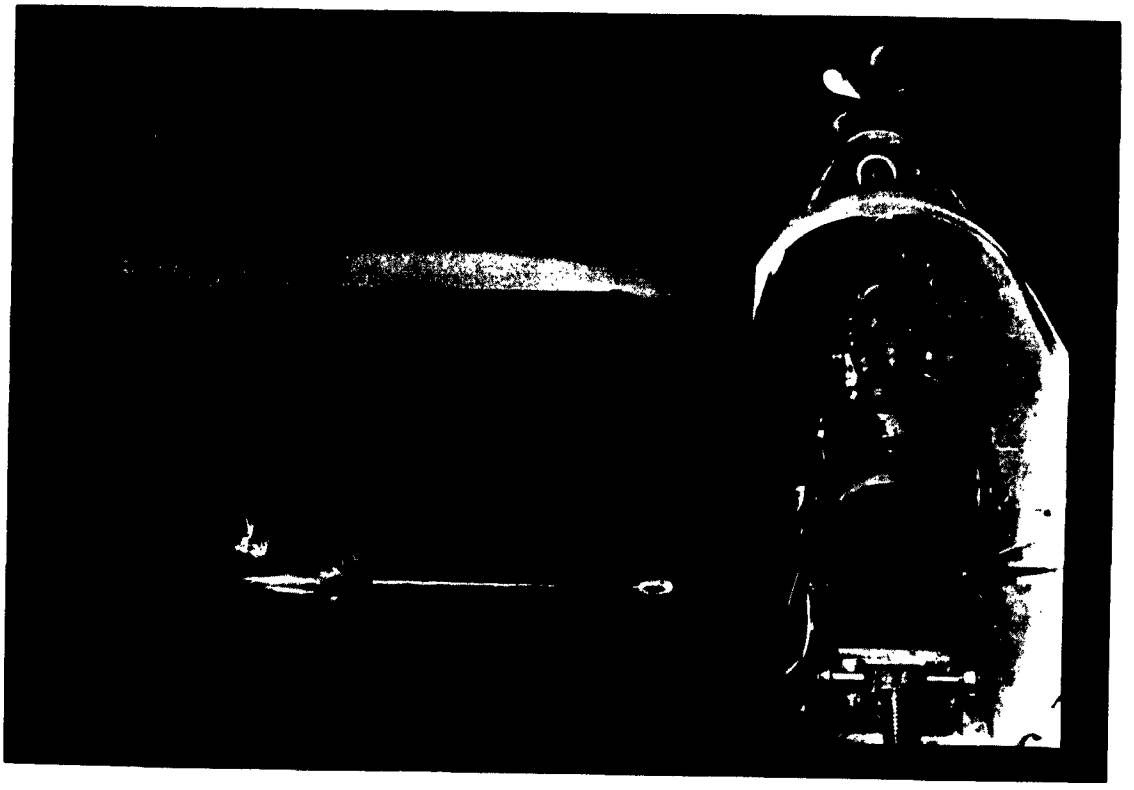

Figure 8 – Model 4620 Equipped for Propulsion Using Propeller 3836

with the sting retracted. No measurable change in the residual-resistance coefficient C_r was detected. However, it is believed that the total drag would change in proportion to the wetted area added by the sting, but this is negligibly small, and, therefore, the propulsive coefficient can be used as a powering criterion instead of shaft horsepower.

Open-water characteristic curves for Propeller 3836 are shown in Figure 25 of Appendix E. For $L_0/D = 0.6$, the corresponding design thrust and speed coefficients, K_t and J, are 0.192 and 1.292, respectively. Figure 25 shows that Propeller 3836 is operating at practically maximum efficiency for $J = 1.292$. The experimental propeller efficiency is shown in Figure 6 for Propeller 3836. Based on these data, the agreement between the predicted propeller performance and the experimental result is good. The only additional determination made from the open-water data is the effective wake fraction as derived from the usual Froude synthesis.

Turning now to the propulsion problem, first compare the hull efficiency quantities $(1-t)$ and $(1-W)$ which were obtained by experiment and by computation. The results of the submerged propulsion test are given in Figure 9 as curves of the various propulsion coefficients versus the total resistance coefficient. Figure 9 is entered at the indicated design J with the following result: $(1-t) = 1.00$ and $(1-W) = 0.85$. Using the faired values, $(1-t) = 0.98$ from Figure 3 and $(1-W_{0.7}) = 0.84$ from Figure 5, it is found that the computed and experimental hull

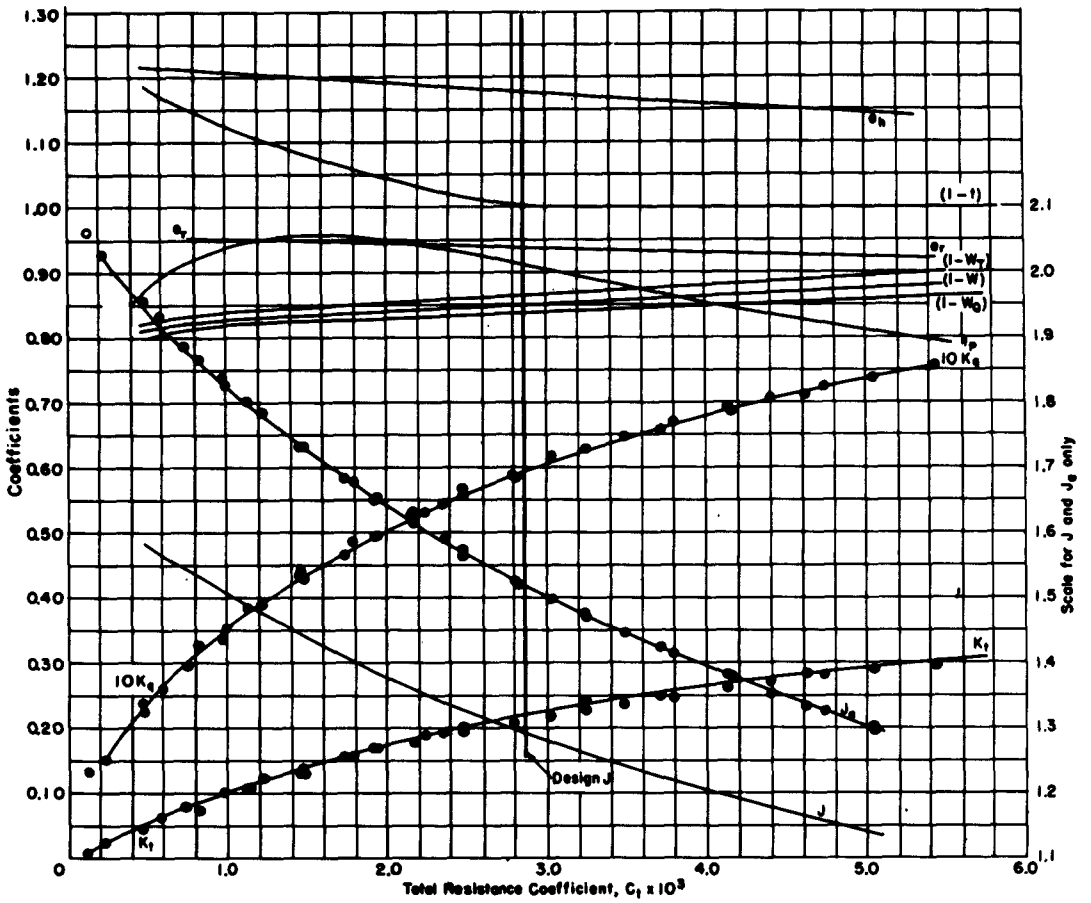

Figure 9 – Submerged Propulsion Test with Propeller 3836

efficiency quantities are in close agreement. This close agreement between the computed and experimental results for the hull efficiency is considered an important consequence of this study. The experimental curve of η_p in Figure 9 was determined directly from measured values of model resistance and propeller power. Although the e_r curve of Figure 9 was calculated as a derived quantity, the experimental value $e_r = 0.94$ at design J compares well to a computed value $e_r = 0.95$ from Equation [1] and [1a]. The experimental value of η_p is about 0.91 at design J. This value is plotted in Figure 7 at $L_0/D = 0.6$, where it is seen to lie on the computed curve.

CONCLUDING REMARKS

The effect on the propulsion quantities, thrust deduction, wake, propeller efficiency, and propulsive coefficient of variations in body-propeller axial clearance at deep submergence on a body of revolution Series 58 form was determined. Some principal findings which have

resulted from this study are: (1) The pressure field due to propeller action is significant for approximately the last 20 percent of the body length, and the thrust-deduction coefficient is essentially zero for body-propeller clearances (measured from a reference station at 0.966 of the body length) greater than the maximum diameter of the body. (2) A rather flat curve of propulsive coefficient versus body-propeller clearance was calculated, but a modest increase of several points in propulsive coefficient might be possible if the propeller is located at about 0.6 diameters behind the reference station. For the condition investigated, the experimental results are in good agreement with the computed values. For example, at a body-propeller clearance of 0.6 maximum body diameters comparative results were obtained as follows:

Quantity	Computed	Experiment
Thrust deduction factor	0.98	1.00
Wake factor	0.84	0.85
Propeller open-water efficiency	0.82	0.82
Relative rotative efficiency	0.95	0.94
Propulsive coefficient	0.91	0.91

Although the foregoing discussion has dealt with propeller location in connection with powering aspects of a bare hull, the need for collateral information on vibration, cavitation, and noise is emphasized. For example, in a circumferentially nonuniform wake, the wake peaks are diminished by increasing the axial clearance between an appendage configuration and the propeller. Two possible outcomes of increased clearance are (1) improved propeller cavitation and noise characteristics, and (2) lower fluctuating thrust amplitudes. An additional improvement which might occur as a result of increased hull-propeller clearance is a reduction of surface forces due to hydrodynamic pressure fluctuations.[11] This is an important problem in connection with vibration and noise.

ACKNOWLEDGMENTS

The helpful suggestions and encouragement given by Dr. W.L. Haberman and Dr. W.B. Morgan, particularly in connection with the theoretical aspects of the work, are greatly appreciated. Also, the author wishes to express his thanks to all personnel of the Ship Powering Division who participated in the conduct of the experiments.

APPENDIX A

GEOMETRICAL DATA AND PHOTOGRAPH OF MODEL 4620

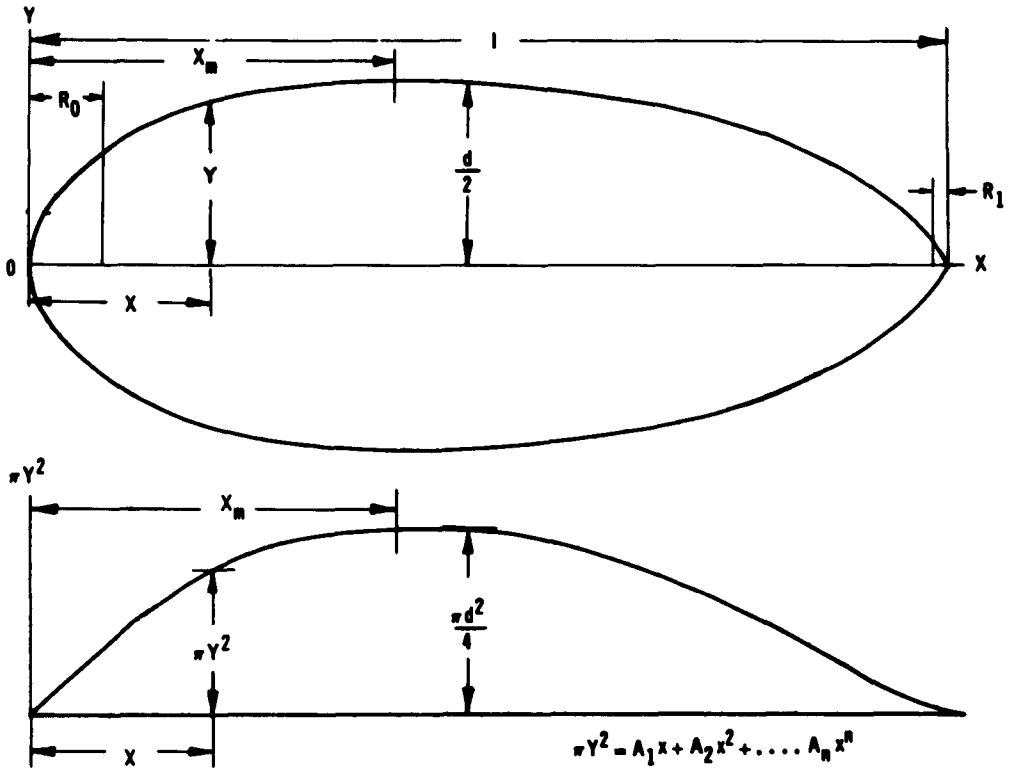

Figure 10 – Principal Dimensions of a Body of Revolution and Its Sectional Area Curve

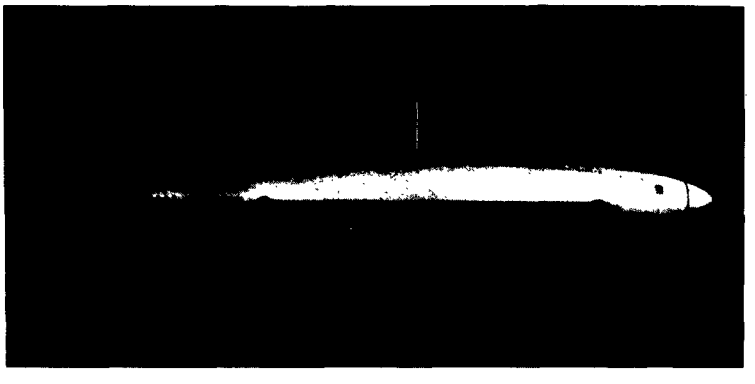

Figure 11 – Model 4620 Equipped with Wake Survey Rakes

TABLE 2

Offsets and Particulars for Model 4620

X in.	*Y* in.	*X* in.	*Y* in.
0.0	0.0	93.6	11.82
3.6	3.5	97.2	11.66
7.2	4.977	100.8	11.49
10.8	6.108	104.4	11.29
14.4	7.047	108.0	11.07
18.0	7.850	111.6	10.83
21.6	8.549	115.2	10.56
25.2	9.160	118.8	10.27
28.8	9.697	122.4	9.954
32.4	10.17	126.0	9.613
36.0	10.58	129.6	9.243
39.6	10.93	133.2	8.843
43.2	11.24	136.8	8.411
46.8	11.50	140.4	7.945
50.4	11.71	144.0	7.447
54.0	11.89	147.6	6.910
57.6	12.03	151.2	6.334
61.2	12.13	154.8	5.715
64.8	12.21	158.4	5.053
68.4	12.25	162.0	4.344
72.0	12.27	165.6	3.584
75.6	12.25	169.2	2.774
79.2	12.21	172.8	1.908
82.8	12.15	176.4	0.984
86.4	12.06	180.0	0.0
90.0	11.97		

Model Particulars:

Length, ft	**= 15.0**
Diameter, ft	**= 2.044 (24.53 in.)**
Nose radius, ft	**= 0.1392 (1.670 in.)**
Tail radius, ft	**= 0.0**
Wetted surface, ft^2	**= 70.55**
Volume, ft^3	**= 29.53**
LCB, ft	**= 6.6840**

APPENDIX B

INSTRUMENTATION AND TEST PROCEDURE

WAKE SURVEYS

Because of the flow symmetry without appendages a 3-dimensional flow survey was felt to be unnecessary and, consequently, the arrangement of cylindrical total head and static head tubes shown in Figures 12 and 13 was used. Six transverse surveys were made; the longitudinal position of each plane of measurement was as follows: $L_0/D = 0$, $L_0/D = 1/8$, $L_0/D = 1/4$, $L_0/D = 1/2$, $L_0/D = 1.0$, and $L_0/D = 1.5$. Except for $L_0/D = 0$, the surveys extend radially to $R/R_B = 0.53$, where $R_B = 1.022$ feet. At Station $L_0/D = 0$, a spacer block inserted at the mounting head increased R/R_B to 0.571. This adjustment was made to provide a minimum clearance of four tube diameters between the hull surface and the innermost pitot tube. The entire pressure-measuring system consisted of the pitot rakes as the sensing device and straight tube manometers for the measuring element. The use of water as the metering fluid allowed an accuracy of about 0.15 percent of stagnation pressure to be obtained at the model test speed of 8 knots.

The pitot rakes were connected to straight-tube manometer boards mounted on the towing carriage. A large capacity vacuum tank was connected in parallel to a manifold located at the top of each board, and a suitable vacuum was applied to each manifold to establish a board level. A reference tank partially filled with water and open to atmospheric pressure was connected to a reference tube on each manometer board. A horizontal datum line was formed by the zero reading (model at rest) of each tube. For each board, the difference between the reference tube zero reading and the reference reading at the equilibrium

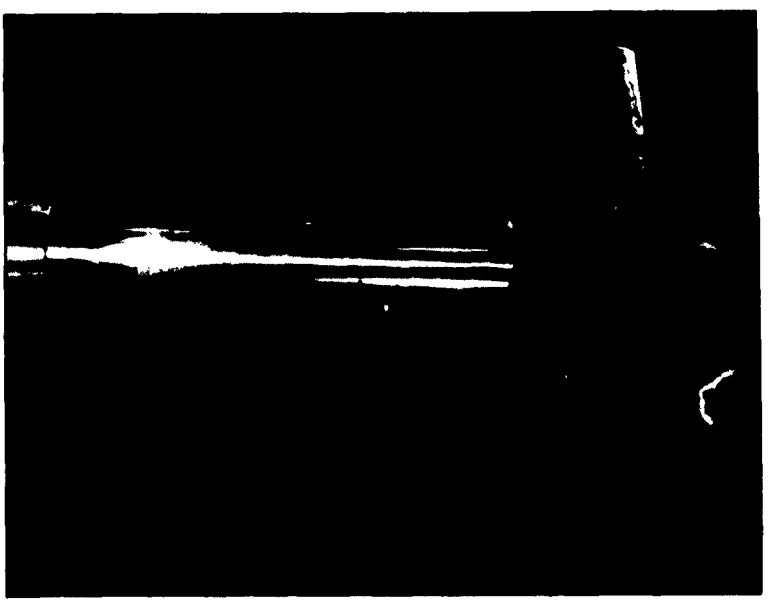

Figure 12 – Pitot Rakes as Mounted on Model 4620

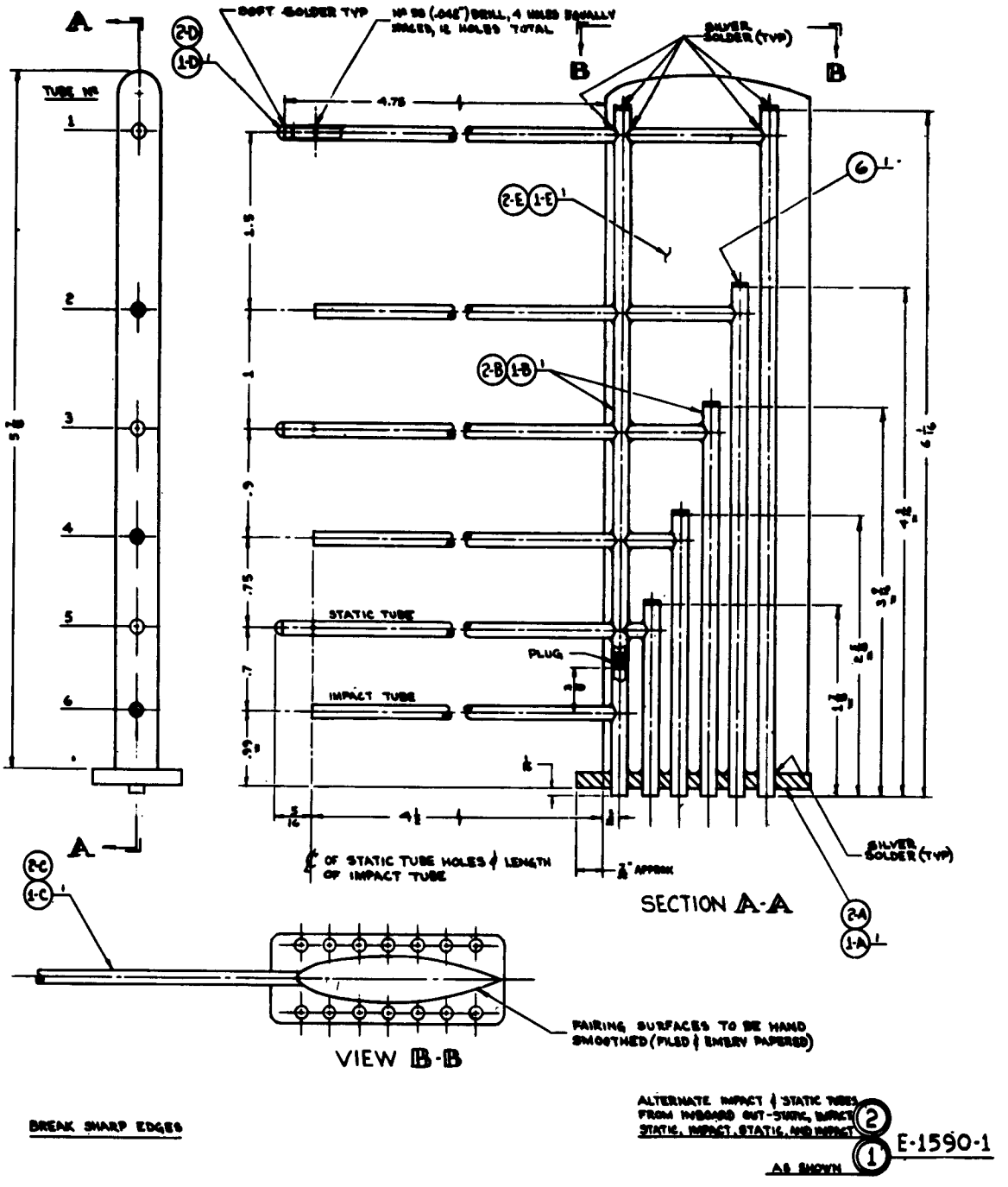

Figure 13 – Details of Starboard Pitot Rake

run was applied as a correction to the datum line, to account for the effect on the zero readings of vacuum changes in the system. The equilibrium run was determined by observing the maximum or minimum heads attained from a series of constant speed runs. Normally, about five runs were necessary to reach equilibrium. Opening and closing the valves of each tube was accomplished by actuating a solenoid valve immediately after and before the acceleration and deceleration parts of a run, respectively.

RESISTANCE AND POWERING EXPERIMENTS

Resistance tests were conducted by towing the model with the single strut and internal resistance dynamometer arrangement shown by Figure 14. With the model still rigged on the single strut, propulsion tests using a submersible motor and propulsion dynamometer were made immediately following the resistance test. This procedure ensured the same orientation and condition of the model for the two tests. Both resistance and propulsion tests were conducted with a turbulence-stimulating sand strip placed around the girth of a body section at 1/20 of the body length. When necessary, appropriate corrections were applied to the drag data for towing-strut interference effects and for the parasitic drag of the sand strip. The submerged propulsion tests were conducted at constant model speed. Test speeds of 6 and 8 knots were selected in order to cover the desired range of propeller loading within the limits of dynamometer capacity. The propeller was driven by a 5-hp motor and a transmission-type dynamometer, with a capacity of 100 lb of thrust and 100 in-lb of torque, placed between the propeller and the driving motor.

In essence, the various propulsion quantities are obtained as functions of C_s much in the same manner as open-water propeller characteristics are obtained as functions of J. In both cases the data are expressed as functions of load.

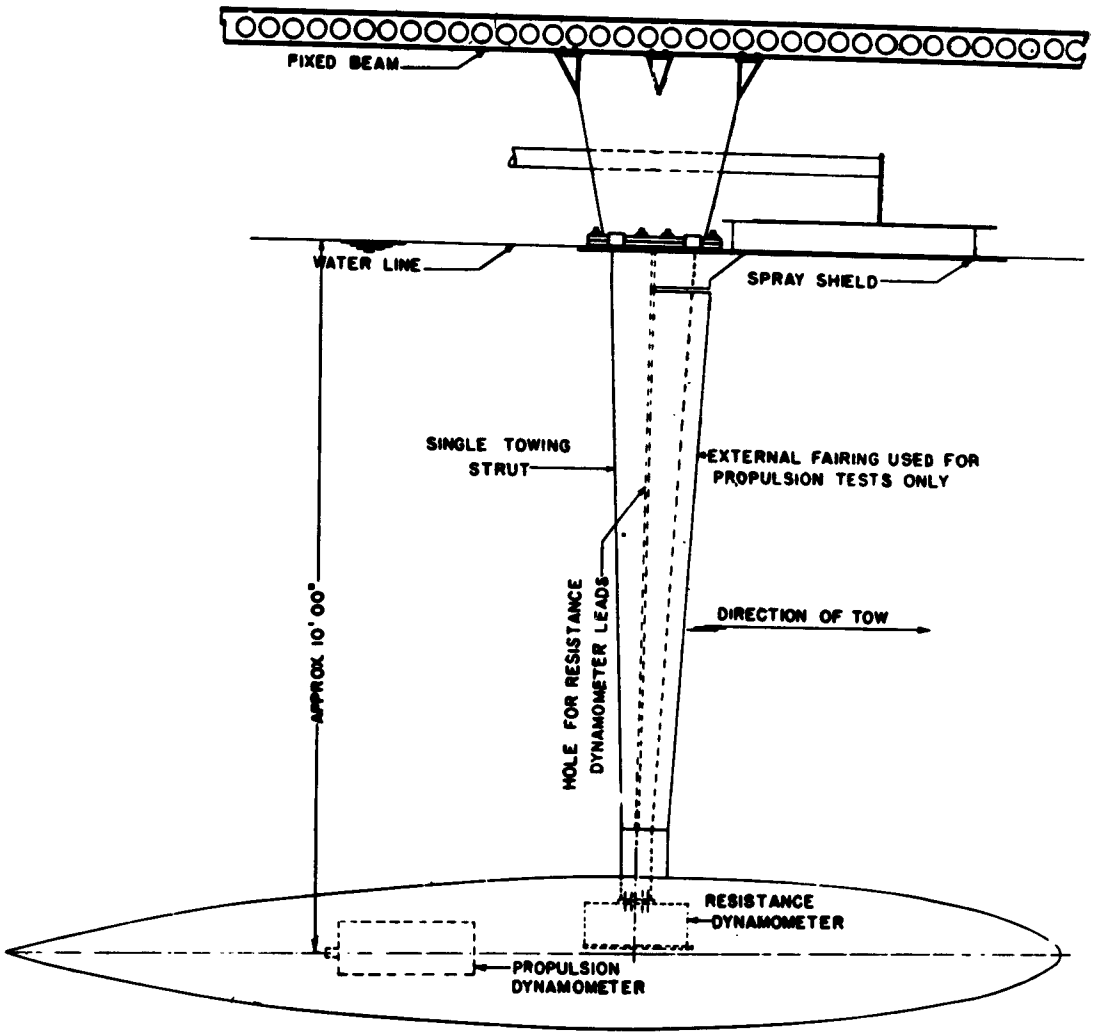

Figure 14 – Schematic Diagram of Arrangement of Model-Towing Apparatus

APPENDIX C

DATA FOR USE IN COMPUTING THRUST DEDUCTION FOR MODEL 4620

THRUST DEDUCTION COMPUTATIONS

The nondimensional disturbing velocities v_r/u_a and v_θ/u_a, where u_a is the propeller-induced velocity at infinity due to a cylindrical vortex sheet* of ring vortices, are given as functions of the spherical coordinates r/R and θ in Reference 1. These velocities are used to obtain the velocity ratio U/V. The procedure for calculating U/V is outlined briefly. A radial distribution of thrust or circulation required for the calculation of thrust deduction for a wake-adapted propeller can be approximated by an equivalent rectangular distribution. Consistent with this approximation and the characteristics of the mathematical model of the propeller (i.e., infinite number of blades and very small pitch), it has been shown in Reference 1 that the rate of change in the x-direction of the elementary circulation $\frac{\partial \Gamma}{\partial X}$ about a vortex filament is equal to the induced velocity u_a far behind the propeller disk. In other words, the circulation per unit length at a sufficiently large distance behind the propeller disk is u_a. Numerically, write

$$\left(\frac{\partial \Gamma}{\partial X}\right)_{\infty} = u_a$$

From momentum theory,[1] velocity u_a is related to propeller thrust coefficient C_T and the propeller speed of advance V_a by the quadratic equation

$$\left(\frac{u_a}{V_a}\right)^2 + 2\frac{u_a}{V_a} - C_T = 0 \qquad [3]$$

which when solved for u_a/V_a becomes

$$\frac{u_a}{V_a} = -1 + \sqrt{1 + C_T} \qquad [3a]$$

and

$$\frac{u_a}{V} = (1 - W_0)\frac{u_a}{V_a}$$

where V is the body speed and W_0 is the effective wake fraction.

It has been shown[1] that a representative radial thrust distribution is given by a pair of cylindrical vortex sheets, one at $R/R_0 = 0.23$ with a circulation distribution $-\frac{\partial \Gamma}{\partial X}$ and the other at $R/R_0 = 0.85$ with strength $\frac{\partial \Gamma}{\partial X}$. The effective value of C_T is based on the reduced

*This cylindrical vortex sheet is composed of a succession of closely spaced circular vortex filaments which extend to infinity behind the propeller.

area; the ratio r/R, on the reduced radius. The procedure for calculating the velocity ratio U/V is now complete with the finding of u_a/V; it is possible to express all velocities as fractions of the speed V. The pressure coefficients are obtained from the Bernoulli equation

$$\frac{p}{q} = 1 - \left(\frac{U}{V}\right)^2$$

where q is the free-stream stagnation pressure. The thrust-deduction coefficient t is a function of the integral of the difference $\Delta p/q$ between the towed and propelled pressure coefficients calculated for the afterbody. When the pressure coefficient is invariant around the circumference of a section (bare-hull case), it can be shown that

$$t = \frac{T - R_t}{T} = \frac{\Delta R_t}{T} = \frac{\pi D^2 q}{T} \int_a^b \Delta \frac{p}{q} f'(x)dx \qquad [4]$$

where

$$\Delta R_t = (\pi D^2 q)\Delta C_D = \pi D^2 q \int_a^b \Delta \frac{p}{q} f'(x)dx$$

and

$$f'(x) = 2y \frac{dy}{dx} = \frac{1}{\pi D^2} \frac{dA}{dx}$$

The function $f'(x)$ is the slope of the nondimensional sectional area curve.

A Series 58 form[12] (TMB Model 4620) was selected for the computable example and for the experiments. Model particulars are given in Appendix A. A reference station $L_0 = 0$ (see Figure 1 in Analysis), is located at 0.966 of the body length. The function $2y\frac{dy}{dx}$ has been computed for the last 20 percent of the body length, and its values are tabulated in Table 3.

Given the geometry of the body, the thrust deduction coefficient t is computed by using Equation [3a], the propeller nondimensional disturbing velocities v_r/u_a and v_ϕ/u_a, and Equation [4]. The propeller designs for the various longitudinal positions L_0/D are

TABLE 3

Slope of Nondimensional Sectional Area Curve for Series 58 Form, Model 4620

x	$2y\frac{dy}{dx}$
0.80	−0.64078
0.82	−0.63870
0.84	−0.62828
0.86	−0.60792
0.88	−0.57574
0.90	−0.52966
0.92	−0.46741
0.94	−0.38632
0.96	−0.28350
0.98	−0.15590
1.00	0.00000

for a constant thrust T of 82,680 lb. An effective C_T for Equation [3] is calculated for each longitudinal position by obtaining V from the typical resistance curve depicted in Figure 15. In Figure 15 the curve was entered on the ordinate R_t = 82,680 $(1-t)$, where $(1-t)$ was estimated from data of Breslin[2] and available experimental data at $L_0/D \approx 1/8$; see data point in Figure 3. The results of this procedure are summarized as follows:

L_0/D	$(1-t)$	$(1-W_0)^*$	V knots	C_T
0.125	0.920	0.805	30.0	0.5118
0.25	0.950	0.817	30.42	0.4834
0.50	0.978	0.837	30.81	0.4488
1.0	1.00	0.865	31.09	0.4127

*Appropriate values of $(1-W_0)$ were taken from Figure 5.

Since the methods and computer programs available for determining the potential flow at the body surface for the body alone are considered elsewhere,[13] they will not be discussed here.

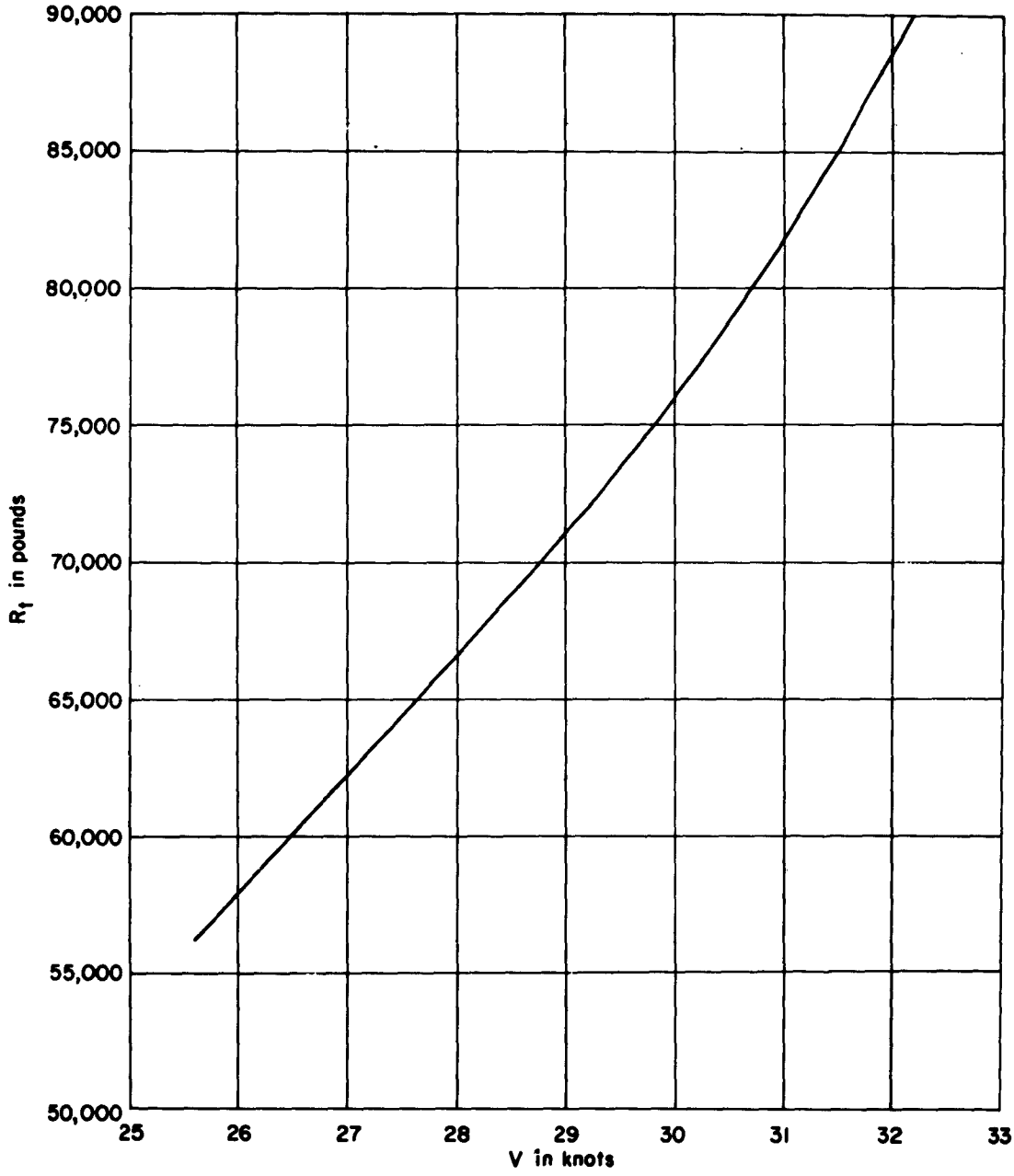

Figure 15 – Typical Resistance Curve

TABLE 4

Computations for Velocity Ratio $\frac{U}{V}$ and Pressure Coefficient $\Delta\frac{p}{q}$ at $\frac{L_0}{D} = \frac{1}{4}$

$$\frac{u_a}{V} = 0.17806$$

1	2	3	4	5	6	7	8	9	10	11	12	13	14
x	y	θ^0	δ^0	$\frac{r}{R}$	$\frac{v_r}{u_a}$	$\frac{v_\theta}{u_a}$	$\frac{v_r}{V}$	$\frac{v_\theta}{V}$	$\frac{u_t}{V}$ Hull	$\frac{u_i}{V}$ Propeller	$\frac{U}{V}$ Total	Total $\frac{p}{q}$	$\Delta\frac{p}{q}$
0.70	0.3919	10.060	5.648	10.558	0.00224	0.000	0.000399	0.000	1.01882	0.000398	1.01922	−0.0388	0.0008
0.80	0.3036	11.628	8.182	7.0871	0.00498		0.000887		1.00000	0.000885	1.00088	−0.0018	0.0018
0.88	0.2060	13.060	10.780	3.9444	0.01607		0.00286		0.9716	0.00286	0.97446	0.0504	0.0056
0.92	0.1461	13.807	12.295	2.8806	0.03012	0.000	0.00536	0.000	0.9487	0.00536	0.95406	0.0898	0.0102
0.96	0.0778	14.496	13.942	1.4625	0.088	0.0075	0.01567	0.001335	0.8944	0.01566	0.91006	0.1718	0.0282
0.98	0.0401	14.583	14.835	0.74940	0.205	0.0250	0.03650	0.004452	0.8031	0.03652	0.83962	0.2950	0.0600

Column:

1. $x = \frac{X}{L}$
2. $y = \frac{Y}{D}$
3. arc tan $\frac{D}{L}\left(\frac{y}{x_1 - x}\right)$, x_1 denotes propeller location
4. arc tan $\frac{D}{L}\frac{f'(x)}{2y}$, Table 3
5. $\frac{r}{R} = k\frac{(x_1 - x)}{\cos\theta}$ where $k = \frac{2}{\frac{R}{R_0}}\left(\frac{D}{d}\right) = 34.536$

6, 7, 8, 9 from Reference 1 and Equation [3a]

10. Calculated from program according to Reference 13
11. $u_i = v_r \cos(\theta - \delta) - v_\theta \sin(\theta - \delta)$
12. Column 10 + Column 11
13. Column 12 and Equation $\frac{p}{q} = 1 - \left(\frac{U}{V}\right)^2$
14. Column 13 − Column 10 and Equation $\frac{p}{q} = 1 - \left(\frac{u_t}{V}\right)^2$

TABLE 5

Computations for Velocity Ratio $\frac{U}{V}$ and Pressure Coefficient $\Delta\frac{p}{q}$ at $\frac{L_0}{D} = \frac{1}{2}$

$$\frac{u_a}{V} = 0.1705$$

1	2	3	4	5	6	7	8	9	10	11	12	13	14
x	y	θ^0	δ^0	$\frac{r}{R}$	$\frac{v_r}{u_a}$	$\frac{v_\theta}{u_a}$	$\frac{v_r}{V}$	$\frac{v_\theta}{V}$	$\frac{u_t}{V}$ Hull	$\frac{u_i}{V}$ Propeller	$\frac{U}{V}$ Total	Total $\frac{p}{q}$	$\Delta\frac{p}{q}$
0.80	0.3036	10.025	8.182	8.206	0.0037	0.000	0.0006	0.000	1.0000	0.0006	1.0006	−0.0012	0.0012
0.88	0.2060	10.329	10.780	5.406	0.0086		0.0015		0.9716	0.0015	0.9731	0.0531	0.0029
0.92	0.1461	9.905	12.295	3.996	0.0156		0.0026		0.9487	0.0026	0.9513	0.0950	0.0050
0.96	0.0078	8.152	13.942	2.582	0.030	0.000	0.0051	0.000	0.8944	0.0051	0.8995	0.1909	0.0091
0.98	0.0401	5.777	14.835	1.875	0.060	0.003	0.0102	0.0005	0.8031	0.0101	0.8132	0.3387	0.0163

Column:

1. $x = \frac{X}{L}$
2. $y = \frac{Y}{D}$
3. arc tan $\frac{D}{L}\left(\frac{y}{x_1 - x}\right)$, x_1 denotes propeller location
4. arc tan $\frac{D}{L}\frac{f'(x)}{2y}$, Table 3
5. $\frac{r}{R} = k\frac{(x_1 - x)}{\cos\theta}$ where $k = \frac{2}{\frac{R}{R_0}}\left(\frac{D}{d}\right) = 34.536$

6, 7, 8, 9 from Reference 1 and Equation [3a]

10. Calculated from program according to Reference 13
11. $u_i = v_r \cos(\theta - \delta) - v_\theta \sin(\theta - \delta)$
12. Column 10 + Column 11
13. Column 12 and Equation $\frac{p}{q} = 1 - \left(\frac{U}{V}\right)^2$
14. Column 13 − Column 10 and Equation $\frac{p}{q} = 1 - \left(\frac{u_t}{V}\right)^2$

TABLE 6

Computations for Velocity Ratio $\frac{U}{V}$ and Pressure Coefficient $\Delta\frac{p}{q}$ at $\frac{L_0}{D} = 1$

$\frac{u_a}{V} = 0.16313$

1	2	3	4	5	6	7	8	9	10	11	12	13	14
x	y	θ^0	δ^0	$\frac{r}{R}$	$\frac{v_r}{u_a}$	$\frac{v_\theta}{u_a}$	$\frac{v_r}{V}$	$\frac{v_\theta}{V}$	$\frac{u_t}{V}$ Hull	$\frac{u_i}{V}$ Propeller	$\frac{U}{V}$ Total	Total $\frac{p}{q}$	$\Delta\frac{p}{q}$
0.80	0.3036	7.799	8.182	10.527	0.002256	0.000	0.000368	0.000	1.00000	0.000368	1.0004	−0.0008	0.0008
0.88	0.2060	7.205	10.780	7.7281	0.004186		0.000683		0.9716	0.000682	0.9723	0.0546	0.0014
0.92	0.1461	6.241	12.295	6.3228	0.006254		0.001020		0.9487	0.00100	0.9497	0.0981	0.0019
0.96	0.0778	4.269	13.942	4.9179	0.01034		0.001687		0.8944	0.00166	0.8961	0.1970	0.0030
0.98	0.0401	2.564	14.835	4.2175	0.01406		0.002294		0.8031	0.00224	0.8053	0.3515	0.0035

Column:

1. $x = \frac{X}{L}$
2. $y = \frac{Y}{D}$
3. arc tan $\frac{D}{L}\left(\frac{y}{x_1 - x}\right)$, x_1 denotes propeller location
4. arc tan $\frac{D}{L}\frac{f'(x)}{2y}$, Table 3
5. $\frac{r}{R} = k\frac{(x_1 - x)}{\cos\theta}$ where $k = \frac{2}{R}\left(\frac{D}{d}\right) = 34.536$

6, 7, 8, 9 from Reference 1 and Equation [3a]

10. Calculated from program according to Reference 13
11. $u_i = v_r \cos(\theta - \delta) - v_\theta \sin(\theta - \delta)$
12. Column 10 + Column 11
13. Column 12 and Equation $\frac{p}{q} = 1 - \left(\frac{U}{V}\right)^2$
14. Column 13 − Column 10 and Equation $\frac{p}{q} = 1 - \left(\frac{u_t}{V}\right)^2$

APPENDIX D
WAKE DATA

PITOT RAKE CALIBRATION

The size of the tubes, the radial spacing between tubes, and the form of the fairing are in accordance with design practice; see Appendix B. In contrast to spherical-headed pitot tubes which are sensitive to turbulence it appears that, within the range of the test, Reynolds number has a rather small effect on the readings obtained from a pitot rake of the type used in the present study. Calibration data were obtained at two carriage speeds, 8 and 6 knots. The results of the calibration tests are shown in Figures 16 and 17 where the net impact and the net static heads are plotted versus R for each speed. In the relation

$$V = V_a = C\sqrt{2gh_v}$$

the coefficient C was calculated to be 1.01 for the 6-knot test and 1.006 for the 8-knot test. An average value of $C = 1.008$ was used to reduce all subsequent wake data behind the body.

DISCUSSION OF RESULTS OF WAKE SURVEYS

Free-turbulence shear-flow theory and various similarity hypotheses are not valid in regions of considerable pressure gradients. The wake traverses obtained at the six stations ($L_0/D = 0$ to $L_0/D = 1.5$) are essential to the solution of the problems of this study and will undoubtedly be of additional use in other problems. The original test data for each wake survey showed slight scatter when plotted as curves of total head and static head versus the radius R. Within the limits of test data, the variation of static head with R was linear. For purposes of analysis and discussion, the original data were crossfaired and replotted in nondimensional form in Figures 18, 19, and 20. The most interesting features of the curves shown in Figure 18 are: (1) The asymptotic nature of the wake curves beginning at about $L_0 = D$, and (2) the relatively small change with L_0/D at $R/R_B > 0.5$.

In Figure 19, the variation of the pressure coefficient p/q with L_0/D is shown with R/R_B as a parameter. It is clear from these curves that the static gradient is in the direction of increasing radius; i.e., at each position L_0/D, the velocity is increasing with radius. This, of course, is the expected behavior; however, the real significance of the curves in Figure 19 is the manner in which the p/q curves converge at higher values of L_0/D. At $L_0 = D$, there is very little spread with the parameter R/R_B and at $L_0/D = 1.5$, the static pressure is invariant radially within the range of measurements. One advantage of conducting a wake survey by taking separate measurements of total head and static head is the ability to examine the static gradient and to calculate the potential component of the wake.

CALCULATIONS FOR POTENTIAL WAKE

The streamline wake can be calculated from pitot-static measurements based on the following considerations: (1) The fluid is frictionless, no energy loss occurs, and (2) the model

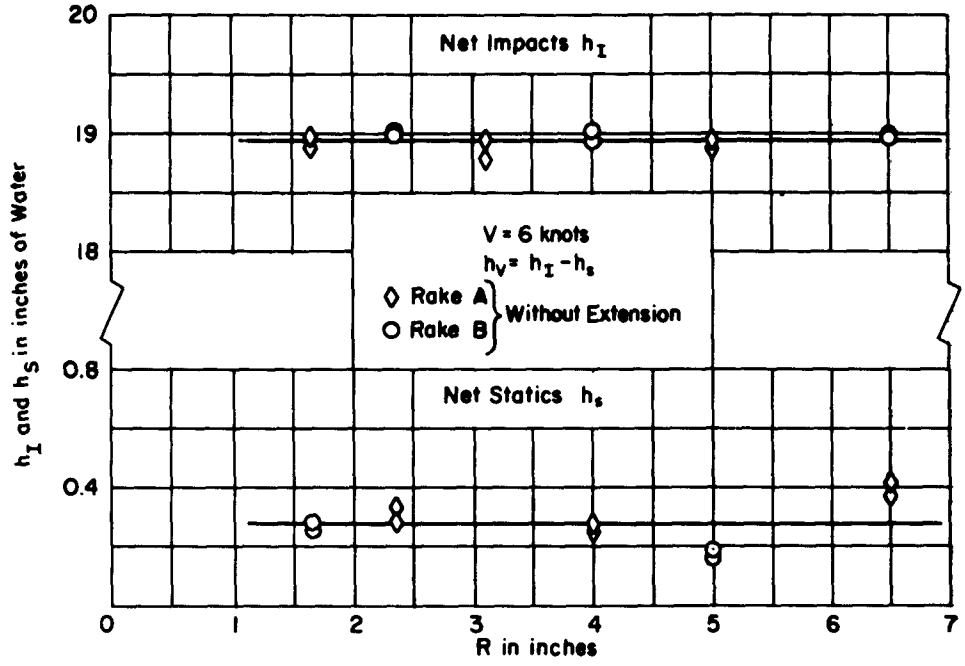

Figure 16 – Pitot Rake Calibration Data at 6 Knots

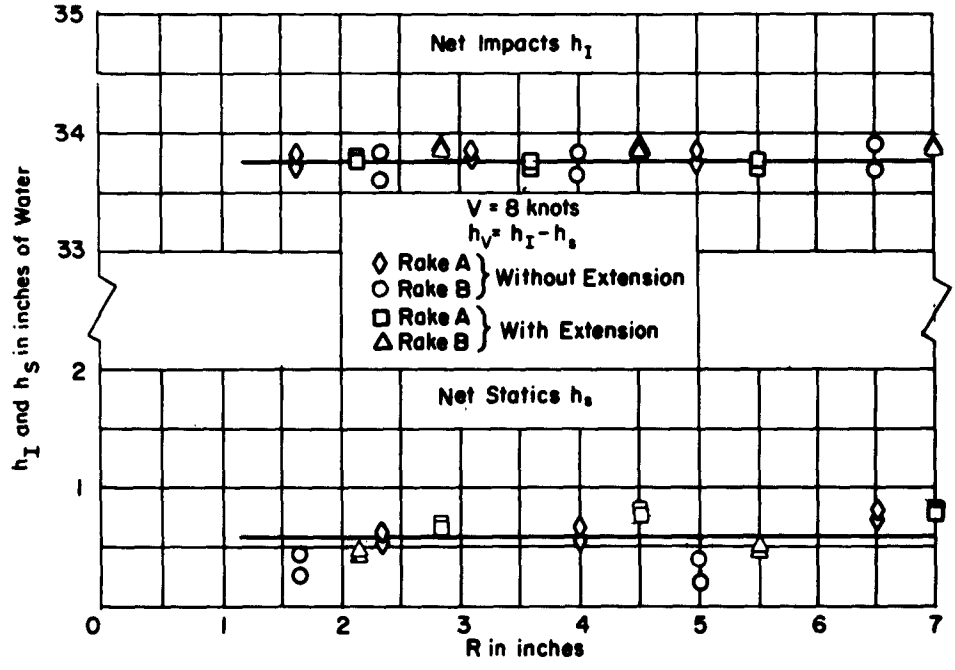

Figure 17 – Pitot Rake Calibration Data at 8 Knots

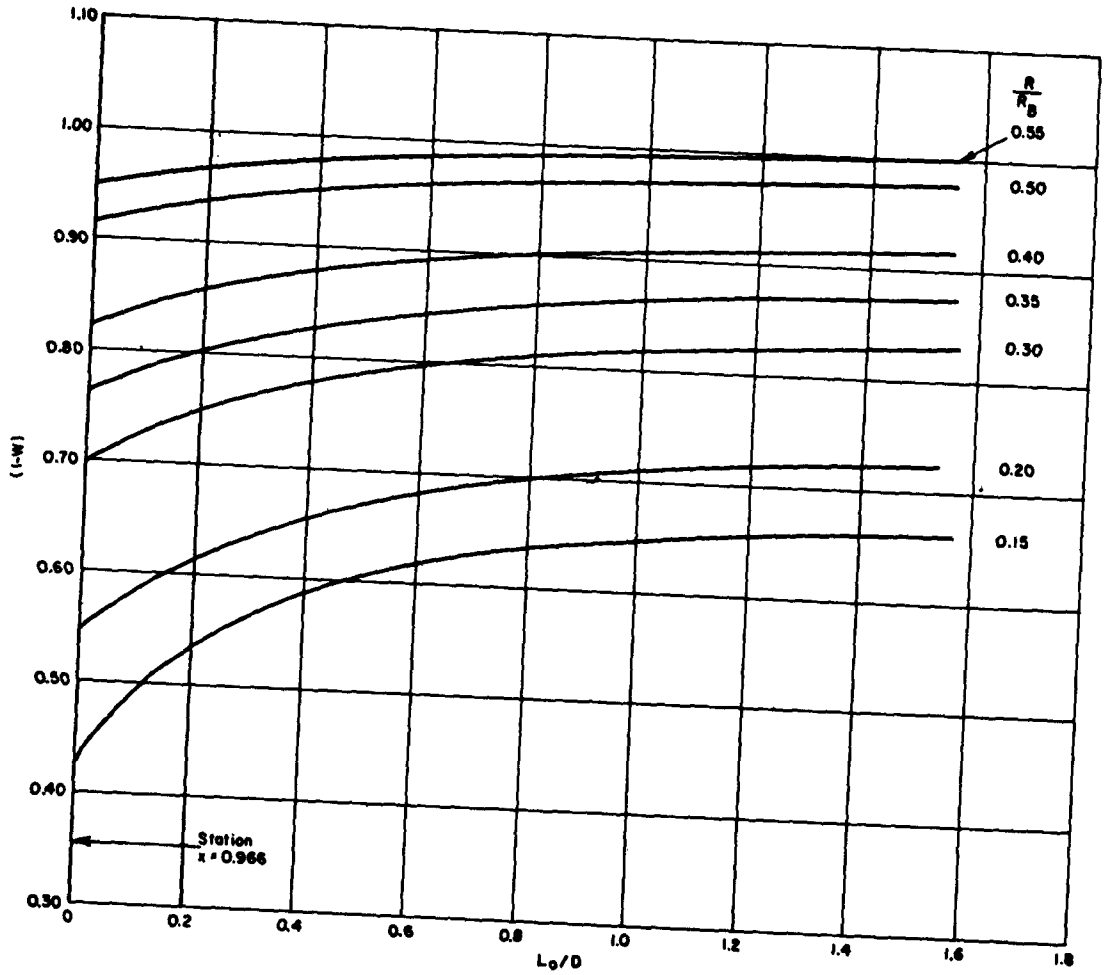

Figure 18 – Distribution of $(1-W)$ as a Function of L_0/D

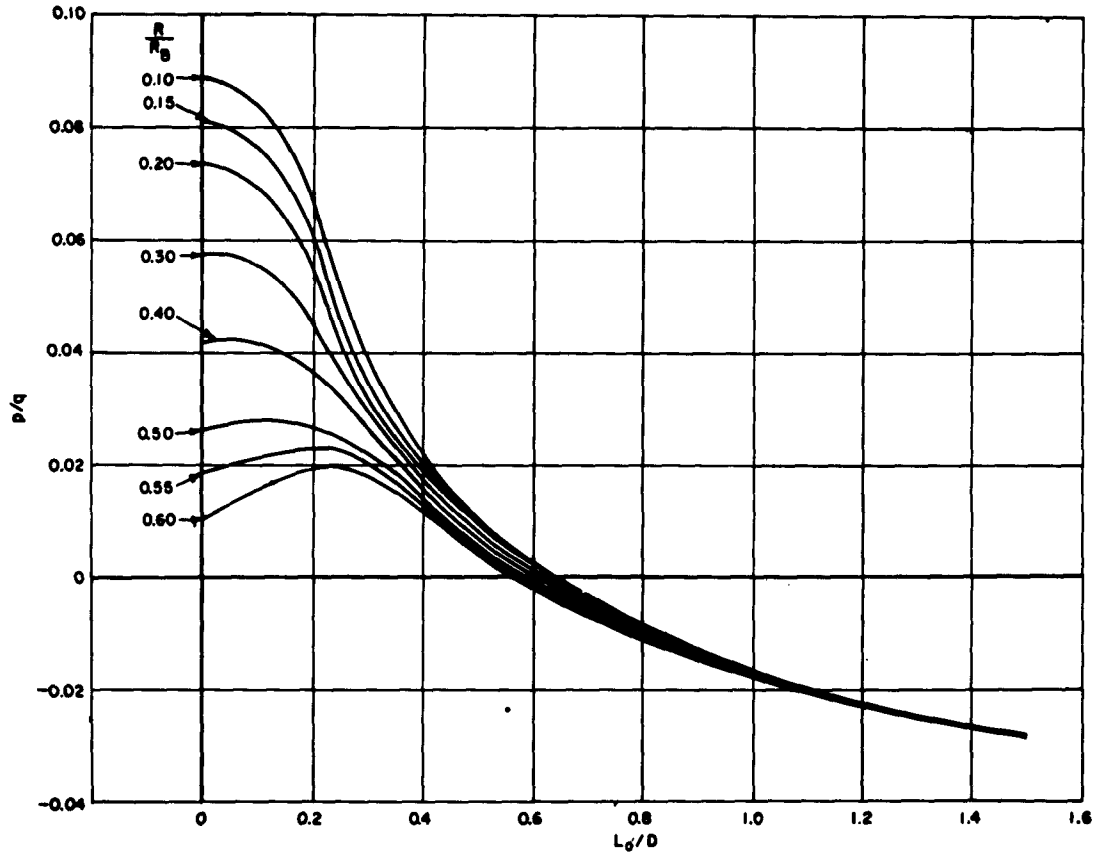

Figure 19 – Distribution of p/q as a Function of L_0/D

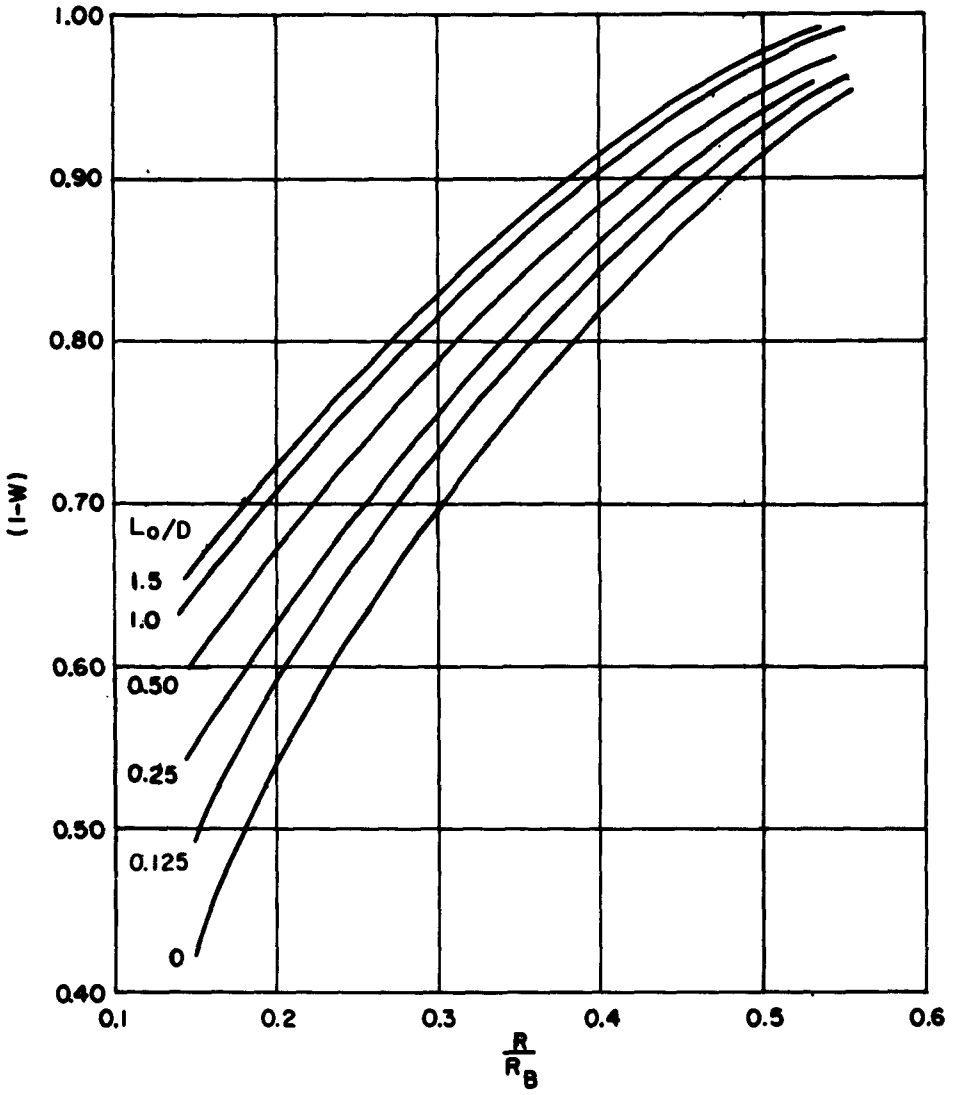

Figure 20 – Distribution of $(1-W)$ as a Function of R/R_B

is steadily advancing in undisturbed water. When $p_\infty = 0$, the Bernoulli constant as measured by a pitot tube at some distance ahead of the model is q so that

$$\tfrac{1}{2}\rho(V - V_p)^2 + p = q \qquad [5]$$

where $V_p = VW_p$, the potential wake velocity. Finally, in terms of the pressure coefficient, the potential velocity ratio becomes

$$1 - W_p = \sqrt{1 - \frac{p}{q}} \qquad [6]$$

Values of $(1 - W_p)$ were calculated from Equation [6] and are plotted in Figure 21a. A slight spread in $(1 - W_p)$ with the parameter R/R_B is observed in the region of $L_0/D < 0.25$. Maximum change in W_p, within the range of the test conditions, is in the order of five points. This corresponds to the small displacement flow associated with well streamlined bodies. The single curve of $(1 - W_p)$ (see Figure 21a) at $L_0/D = 1.5$ will decelerate and approach unity at some greater distance downstream; the total velocity ratio $(1 - W)$ will also become unity, but will not reach free-stream velocity until a much greater distance downstream than the ratio $(1 - W_p)$. In fact, the concept that the potential flow field decays at a greater rate than does the frictional flow field is a basis for speculating that, from the propulsion viewpoint, an optimum propeller location exists.

Figure 21b shows curves of potential velocity ratio for the case of pure streamline flow. This figure also shows that the velocities at equal values of L_0/D are several points lower than those indicated by the comparable curves of Figure 21a. Although the curves of Figure 21b are mostly of academic interest, several points concerning the theoretical calculation of $(1 - W_p)$ deserve discussion. Calculation of a "so-called" potential velocity ratio from experimental measurements is a scheme for resolving the total velocity of a viscous flow into component parts. The procedure followed in the derivation of the curves presented in Figure 21a is really an attempt to evaluate the velocity due only to normal stress. Of course, the wake behind the hull is a free turbulent shear flow. Referring now to Figure 21b, the results shown are for a closed body boundary condition. An exact general method of solving the Neumann problem has been developed for axisymmetric flow. The solution is programmed on a high-speed computer and solutions can be obtained for both closed- and open-body conditions. In an effort to approximate the mathematical representation of the real wake behind the hull, a new body shape with a tail was derived by adding the displacement thickness of the boundary layer to the original body. Agreement with the experimental results was not improved by this process, since one undesirable feature of the body plus tail condition is the exclusion of points close to the centerline behind a body. Of course, the greatest velocity change is within this very region.

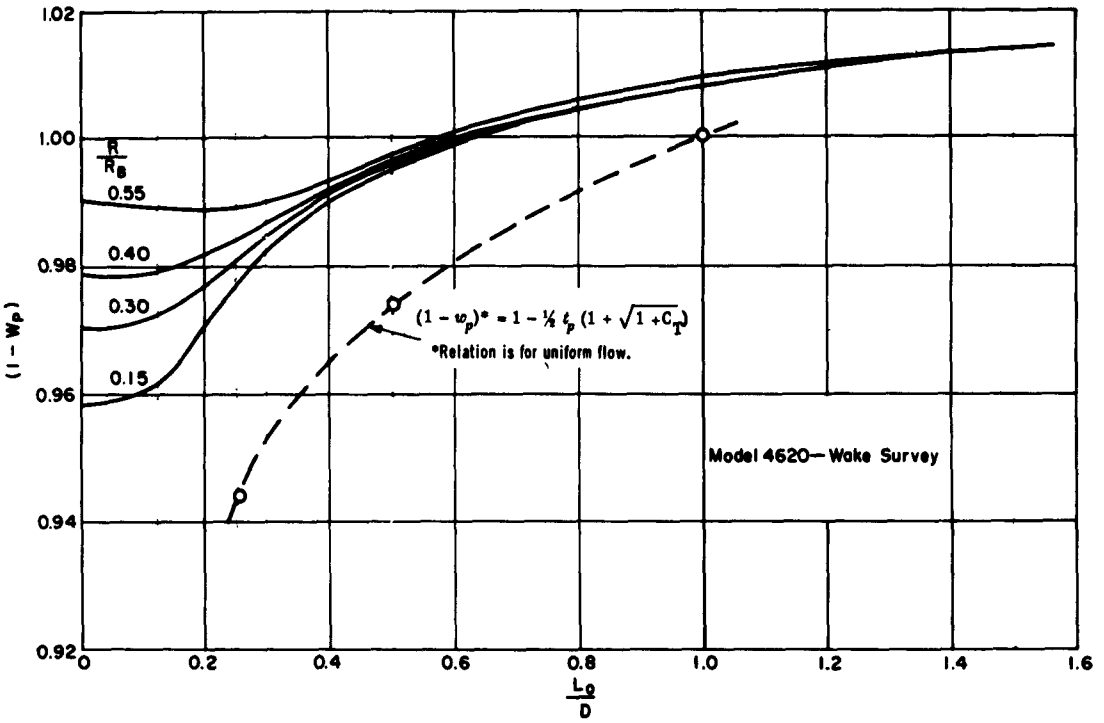

Figure 21a – Experimental

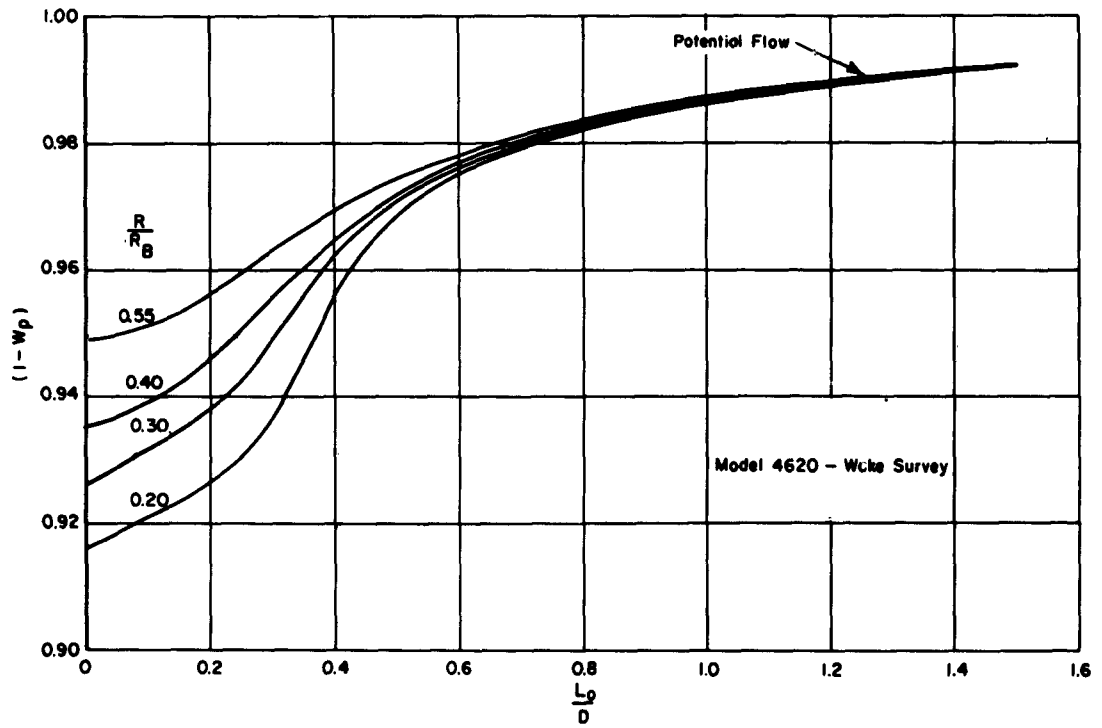

Figure 21b – Theoretical

Figure 21 – Distribution of Potential Velocity Ratio as a Function of L_0/D

APPENDIX E

PROPELLER DATA

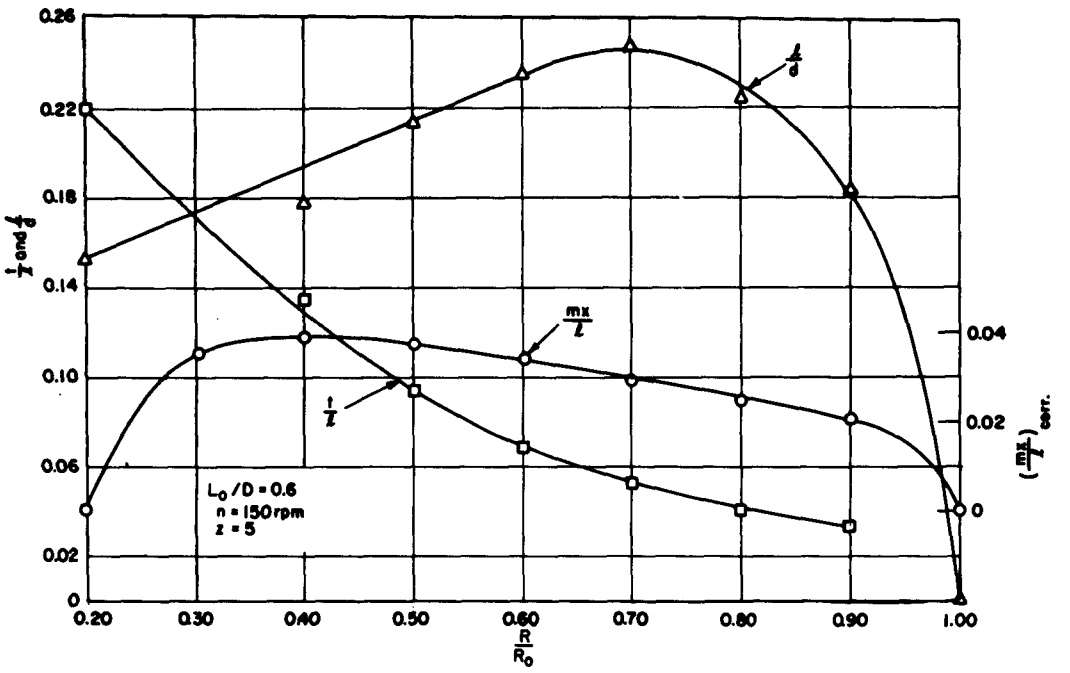

Figure 22 – Blade Geometry of Propeller 3836

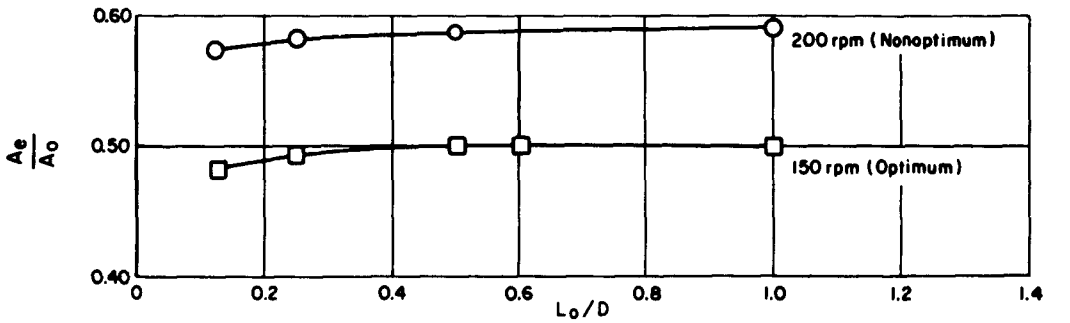

Figure 23 – Expanded-Area Ratio versus L_0/D for Optimum and Nonoptimum Propellers

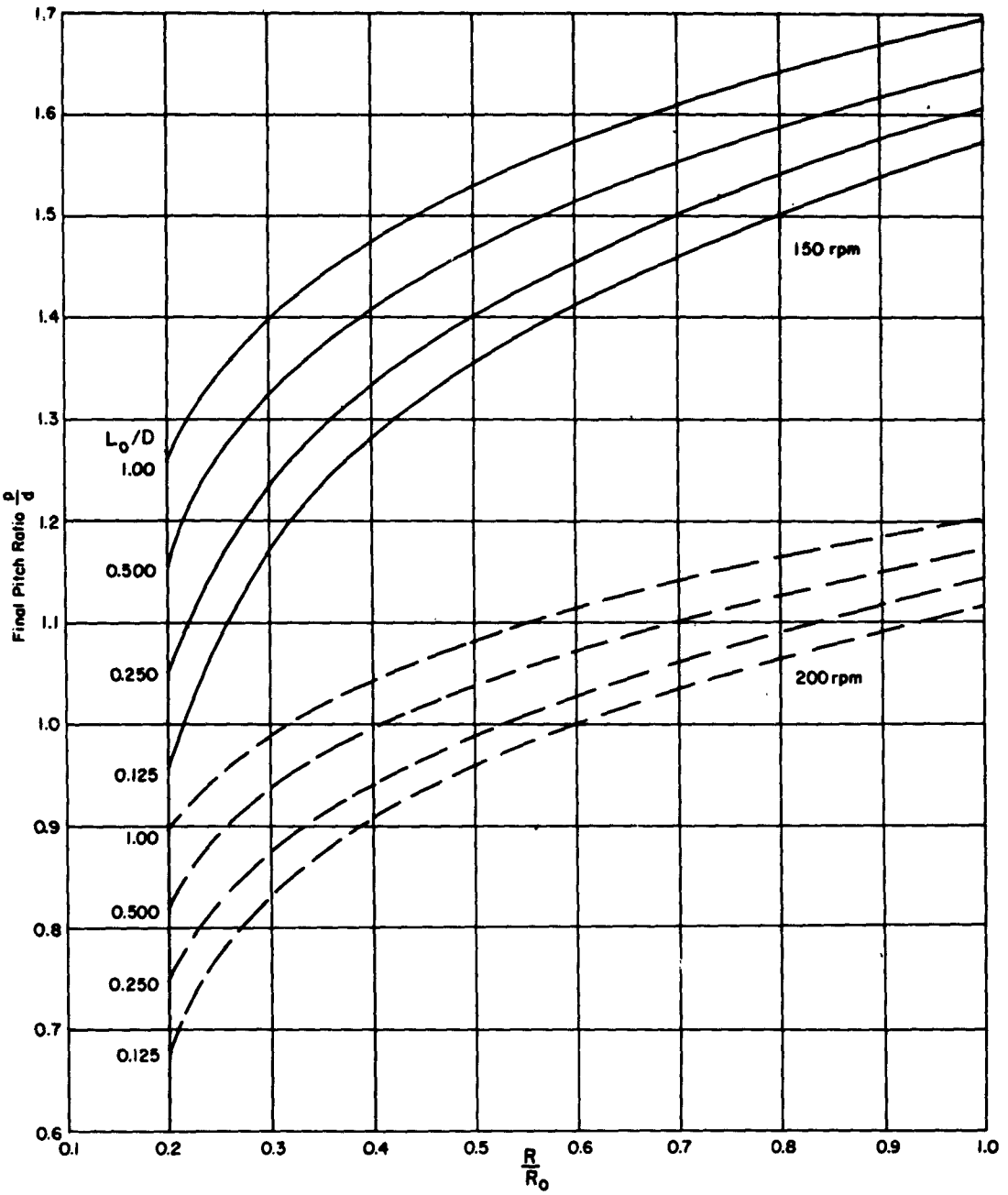

Figure 24 – Final Radial Distribution of Propeller Pitch Ratio for Each Condition

NUMBER OF BLADES	5
EXP. AREA RATIO	0.505
MWR	0.198
BTF	0.042
P/D (AT 0.7R)	1.567
DIAMETER	12.263 in.
PITCH(AT 0.7R)	19.211 in.
ROTATION	R.H.
TEST n	5.6 to 7.0 rps
TEST V_a	3.0 to 12.5 fps

30 MARCH 1960
DAVID W. TAYLOR MODEL BASIN
WASHNGTON, D.C.

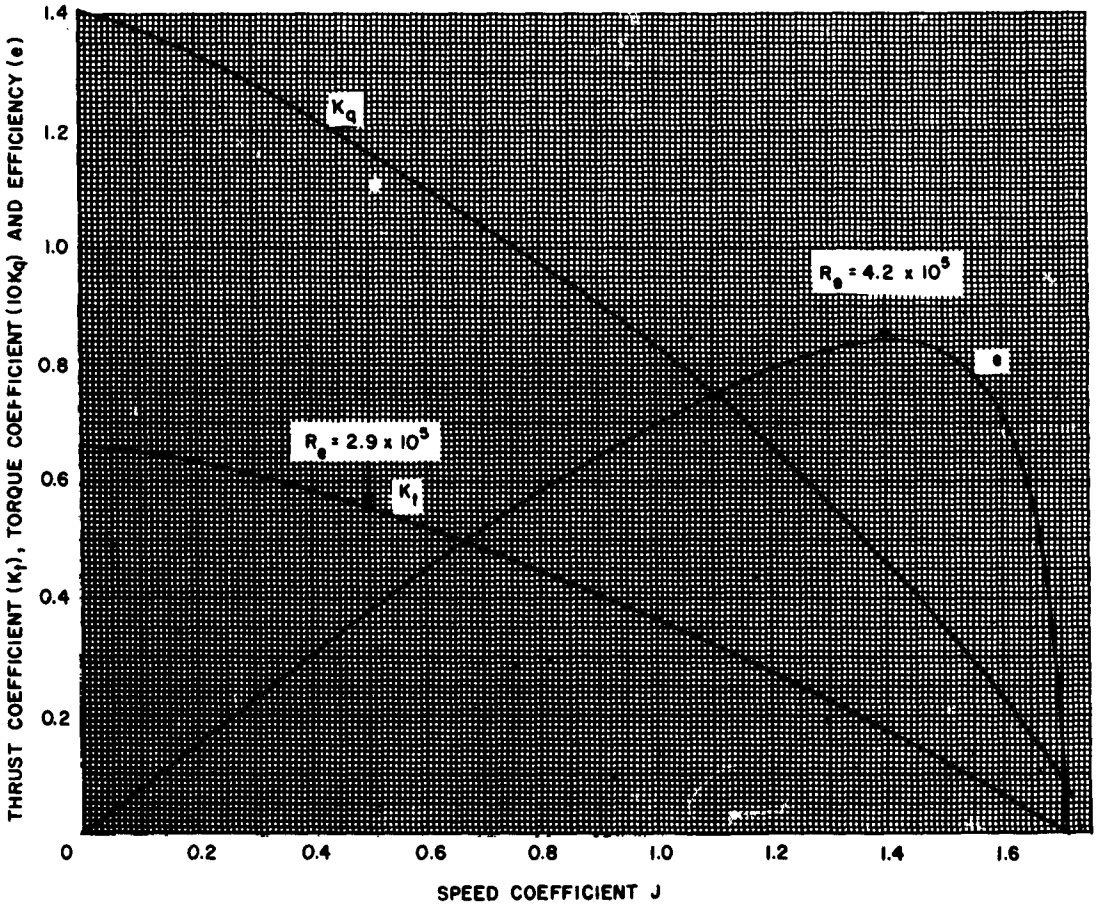

Figure 25 – Open-Water Characteristic Curves for Propeller 3836

REFERENCES

1. Korvin-Kroukovsky, B.V., "Stern Propeller Interaction with a Streamline Body of Revolution," International Shipbuilding Progress, Vol. 3, No. 17 (Jan 1956).

2. Breslin, J.P., "A Simplified Theory for the Thrust Deduction Force on a Body of Revolution," Proceedings 5th Midwestern Conference on Fluid Mechanics (1957).

3. Astrup, N.C., "A Set of Propellers in Open Water and behind a Body of Revolution," Parts 1 and 2, Norwegian Ship Model Experiment Tank Publication Nos. 45 and 46 (1957).

4. Hickling, R., "Propellers in the Wake of an Axisymmetric Body," Institution of Naval Architects, Quarterly Transactions, Vol. 99, No. 4, (Oct 1957).

5. Weinblum, G., "The Thrust Deduction," American Society of Naval Engineers, Vol. 63 (1951).

6. Dickmann, H.E., "The Interaction between Propeller and Ship with Special Consideration to the Influence of Waves," Jahrbuch der Schiffbautechnischen Gesselschaft, 40 (1939).

7. Schoenherr, K.E., and Aquino, A.A., "Interaction between Propeller and Hull," U.S. Experimental Model Basin Report 470 (Mar 1940).

8. Eckhardt, M.K. and Morgan, W.B., "A Propeller Design Method," Transactions Society of Naval Architects and Marine Engineers, Vol. 63 (1955).

9. Gawn, R.W.L., "Effect of Pitch and Blade Width on Propeller Performance," Transactions Institution of Naval Architects, Vol. 95 (1953).

10. Hecker, Richard, "Manual for Preparing and Interpreting Data of Propeller Problems Which Are Programmed for the High-Speed Computers at the David Taylor Model Basin," David Taylor Model Basin Report 1244 (Aug 1959).

11. Tachmindji, A.J. and Dickerson, M.C., "The Measurement of Oscillating Pressure in the Vicinity of Propellers," David Taylor Model Basin Report 1130 (Apr 1957).

12. Landweber, L. and Gertler, M., "Mathematical Formulation of Bodies of Revolution," David Taylor Model Basin Report 719 (Sep 1950).

13. Smith, A.M.O. and Pierce, J., "Exact Solution of the Neumann Problem, Calculation of Non-Circulatory Plane and Axially Symmetric Flows about or within Arbitrary Boundaries," Douglas Aircraft Company Report ES 26988 (Apr 1958).

INITIAL DISTRIBUTION

Copies	
9	CHBUSHIPS 3 Tech Lib (Code 210L) 1 Lab Mgt (Code 320) 2 Prelim Des Br (Code 420) 1 Mach, Sci, & Res Sec (Code 436) 1 Sub Br (Code 525) 1 Prop, Shaft, & Bear Br (Code 644)
5	CHBUWEPS 2 Tech Lib (DL 1-3) 1 Fluid Mech & Flight Dyn Sec (RRRE-4) 1 Supporting Res Br (RUTO-3) 1 RUTO-32 Attn: Mr. H. Eggers
3	CHONR 1 Fluid Dyn Br (Code 438) 1 Struc Mech Br (Code 439) 1 Undersea Programs (Code 466)
1	CDR, USNOL
1	DIR, USNRL
1	CO & DIR, USNEES
1	CDR, USNOTS, Pasadena
1	DTMB High-Speed Phenomena Div Langley Field
1	SUPT USNAVPGSCOL
1	NAVSHIPYD PTSMH
1	NAVSHIPYD MARE
1	O in C, USN Sub School Attn: Sub Dept
1	O in C, PGSCOL, Webb
1	DIR, Aero Res, NASA
10	CDR, ASTIA
1	Dir Def R & E
1	Hydro Lab, CIT
2	Dept NAME, MIT
1	DIR, St. Anthony Falls Hydrau Lab
1	DIR, ORL Attn: Dr. G.F. Wisliconus
1	DIR, DL, SIT
2	Iowa Inst of Hydrau Res State Univ of Iowa 1 Dr. Hunter Rouse 1 Dr. L. Landweber

Copies	
2	Dept NAME, Univ of Michigan Attn: Prof R.B. Couch
1	Univ of Notre Dame Attn: Dr. A.G. Strandhagen
3	School of Engin Univ of California 1 Prof H.A. Schade 1 Dept of Naval Arch 1 Engr Libr
1	Oceanics, Inc. Attn: Dr. Paul Kaplan, Pres
1	TRG
1	Hydronautics, Inc.
1	Ingalls Shipbldg Corp.
1	New York Shipbldg Corp.
2	Gen Dyn Corp., EB Div.
1	Bethlehem Steel Co., Shipbldg Div., Quincy Attn: Mr. Hollinshead DeLuce
2	Gibbs & Cox, Inc.
1	NNSB & DD CO., Engin Tech Div Attn: Mr. John Kane
1	SNAME Attn: Capt W.N. Landers
1	Douglas Aircraft Co., Inc. Aircraft Div., Long Beach Attn: Mr. John L. Hess
1	Vidya, Inc.

David Taylor Model Basin. Report 1456.
EFFECT OF AXIAL POSITION OF PROPELLER ON THE PROPULSION CHARACTERISTICS OF A SUBMERGED BODY OF REVOLUTION, by John L. Beveridge. Mar 1963. vii, 49p. tables, illus., photos., refs. UNCLASSIFIED

The propulsion performance of a submerged body of revolution was determined when the axial clearance between a stern propeller and the body was varied. Theoretical and experimental results indicate that variations, within the range of investigation, in the longitudinal position of a stern propeller do not critically affect the propulsive coefficient. In addition to these results, calculation of the propellers and the thrust deduction is discussed, and experimental results obtained from numerous wake traverses are presented.

1. Bodies of revolution--Propulsion--Performance
2. Bodies of revolution--Configuration
3. Bodies of revolution--Resistance--Mathematical analysis
4. Bodies of revolution--Model TMB series 58
5. Propellers--Thrust--Performance

I. Beveridge, John L.
II. S-R009 01 01

David Taylor Model Basin. Report 1456.
EFFECT OF AXIAL POSITION OF PROPELLER ON THE PROPULSION CHARACTERISTICS OF A SUBMERGED BODY OF REVOLUTION, by John L. Beveridge. Mar 1963. vii, 49p. tables, illus., photos., refs. UNCLASSIFIED

The propulsion performance of a submerged body of revolution was determined when the axial clearance between a stern propeller and the body was varied. Theoretical and experimental results indicate that variations, within the range of investigation, in the longitudinal position of a stern propeller do not critically affect the propulsive coefficient. In addition to these results, calculation of the propellers and the thrust deduction is discussed, and experimental results obtained from numerous wake traverses are presented.

1. Bodies of revolution--Propulsion--Performance
2. Bodies of revolution--Configuration
3. Bodies of revolution--Resistance--Mathematical analysis
4. Bodies of revolution--Model TMB series 58
5. Propellers--Thrust--Performance

I. Beveridge, John L.
II. S-R009 01 01

David Taylor Model Basin. Report 1456.
EFFECT OF AXIAL POSITION OF PROPELLER ON THE PROPULSION CHARACTERISTICS OF A SUBMERGED BODY OF REVOLUTION, by John L. Beveridge. Mar 1963. vii, 49p. tables, illus., photos., refs. UNCLASSIFIED

The propulsion performance of a submerged body of revolution was determined when the axial clearance between a stern propeller and the body was varied. Theoretical and experimental results indicate that variations, within the range of investigation, in the longitudinal position of a stern propeller do not critically affect the propulsive coefficient. In addition to these results, calculation of the propellers and the thrust deduction is discussed, and experimental results obtained from numerous wake traverses are presented.

1. Bodies of revolution--Propulsion--Performance
2. Bodies of revolution--Configuration
3. Bodies of revolution--Resistance--Mathematical analysis
4. Bodies of revolution--Model TMB series 58
5. Propellers--Thrust--Performance

I. Beveridge, John L.
II. S-R009 01 01

David Taylor Model Basin. Report 1456.
EFFECT OF AXIAL POSITION OF PROPELLER ON THE PROPULSION CHARACTERISTICS OF A SUBMERGED BODY OF REVOLUTION, by John L. Beveridge. Mar 1963. vii, 49p. tables, illus., photos., refs. UNCLASSIFIED

The propulsion performance of a submerged body of revolution was determined when the axial clearance between a stern propeller and the body was varied. Theoretical and experimental results indicate that variations, within the range of investigation, in the longitudinal position of a stern propeller do not critically affect the propulsive coefficient. In addition to these results, calculation of the propellers and the thrust deduction is discussed, and experimental results obtained from numerous wake traverses are presented.

1. Bodies of revolution--Propulsion--Performance
2. Bodies of revolution--Configuration
3. Bodies of revolution--Resistance--Mathematical analysis
4. Bodies of revolution--Model TMB series 58
5. Propellers--Thrust--Performance

I. Beveridge, John L.
II. S-R009 01 01